Available online at www.sciencedirect.com
SCIENCE DIRECT®
Geochimica et Cosmochimica Acta 70 (2006) 562–582
Geochimica
www.elsevier.com/locate/gca

Effects of substrate structure and composition on the structure, dynamics, and energetics of water at mineral surfaces: A molecular dynamics modeling study

Jianwei Wang [a,*], Andrey G. Kalinichev [a,b], R. James Kirkpatrick [a,b]

[a] *Department of Geology, University of Illinois at Urbana-Champaign, Urbana, IL 61801, USA*
[b] *NSF Water CAMPwS, University of Illinois at Urbana-Champaign, Urbana, IL 61801, USA*

Received 24 January 2005; accepted in revised form 13 October 2005

Abstract

Molecular dynamics computer simulations of the molecular structure, diffusive dynamics and hydration energetics of water adsorbed on (0 0 1) surfaces of brucite $Mg(OH)_2$, gibbsite $Al(OH)_3$, hydrotalcite $Mg_2Al(OH)_6Cl\cdot 2H_2O$, muscovite $KAl_2(Si_3Al)O_{10}(OH)_2$, and talc $Mg_3Si_4O_{10}(OH)_2$ provide new insight into the relationships between the substrate structure and composition and the molecular-scale structure and properties of the interfacial water. For the three hydroxide phases studied here, the differences in the structural charge on the octahedral sheet, cation occupancies and distributions, and the orientations of OH groups all affect the surface water structure. The density profiles of water molecules perpendicular to the surface are very similar, due to the prevalent importance of H-bonding between the surface and the water and to their similar layered crystal structures. However, the predominant orientations of the surface water molecules and the detailed two-dimensional near-surface structure are quite different. The atomic density profiles and other structural characteristics of water at the two sheet silicate surfaces are very different, because the talc (0 0 1) surface is hydrophobic whereas the muscovite (0 0 1) surface is hydrophilic. At the hydrophilic and electrostatically neutral brucite and gibbsite (0 0 1) surfaces, both donating and accepting H-bonds from the H_2O molecules are important for the development of a continuous hydrogen bonding network across the interfacial region. For the hydrophilic but charged hydrotalcite and muscovite (0 0 1) surfaces, only accepting or donating H-bonds from the water molecules contribute to the formation of the H-bonding network at the negatively and positively charged interfaces, respectively. For the hydrophobic talc (0 0 1) surface, H-bonds between water molecules and the surface sites are very weak, and the H-bonds among H_2O molecules dominate the interfacial H-bonding network. For all the systems studied, the orientation of the interfacial water molecules in the first few layers is influenced by both the substrate surface charge and the ability by the surfaces to facilitate H-bond formation. The first layer of water molecules at all surfaces is well ordered in the *xy* plane (parallel to the surface) and the atomic density distributions reflect the substrate crystal structure. The enhanced ordering of water molecules at the interfaces indicates reduced orientational and translational entropy. In thin films, water molecules are more mobile parallel to the surface than perpendicular to it due to spatial constraints. At neutral, hydrophilic substrates, single-monolayer surface coverage stabilizes the adsorbed water molecules and results in a minimum of the surface hydration energy. In contrast, at the charged and hydrophilic muscovite surface, the hydration energy increases monotonically with increasing water coverage over the range of coverages studied. At the neutral and hydrophobic talc surface, the adsorption of H_2O is unfavorable at all surface coverages, and the hydration energy decreases monotonically with increasing coverage.

1. Introduction

Interaction between water and solid surfaces can substantially affect the properties of both phases, including the structure and dynamics of the near surface water and the

* Corresponding author. Present address: Department of Geology, University of California at Davis, One Shields Avenue, Davis, CA 95616, USA. Fax: +1 530 752 0951.
E-mail address: jwwang@ucdavis.edu (J. Wang).

0016-7037/$ - see front matter © 2005 Elsevier Inc. All rights reserved.
doi:10.1016/j.gca.2005.10.006

reactivity and functionality of the substrate surface (Thiel and Madey, 1987; Hochella and White, 1990; Brown, 2001; Henderson, 2002). These interactions are, thus, of significant interest in many geochemical, technological and biological systems. In geochemistry and environmental science, water–mineral interactions are important factors controlling such processes as surface ion adsorption and ion exchange, which are crucial for the mobility of contaminants in surface and groundwater systems, weathering, soil development, soil moisture behavior, water composition and quality, and removal and sequestration of atmospheric CO_2 (Davis and Kent, 1990; Hochella and White, 1990; Brown et al., 1999; Brown, 2001; Brown and Parks, 2001). Mineral–water interactions are largely controlled by the substrate structure, composition, and surface charge distribution, which vary widely among minerals. The substrate surface structure provides the basic framework for water adsorption. Local variation of near-surface structural charge (electron density) due to structural substitutions or defects provides negatively or positively charged surface sites which can orient the H_2O dipoles and which can significantly influence formation of donating or accepting hydrogen bonds with the surface.

For the common oxides, hydroxides and silicates of the Earth's near-surface environment, the surface chemistry is strongly affected by the pH-dependent surface protonation/deprotonation (Davis and Kent, 1990; Hochella and White, 1990; Brown, 2001; Rustad, 2001). For a given mineral, the bulk properties of the near-surface aqueous solutions, such as pH, can affect the structure and properties of the interfacial water by modifying the substrate surface (Du et al., 1994; Yeganeh et al., 1999; Ostroverkhov et al., 2004). For water on sapphire (Al_2O_3) (Yeganeh et al., 1999) and crystalline or fused quartz (SiO_2) (Du et al., 1994; Ostroverkhov et al., 2004) surfaces, sum frequency vibrational spectroscopy suggests that the H_2O dipoles flip 180° when the solution pH crosses the iso-electric point of the surface. At the water–quartz interface at both low (~2) and high (~12) pH, interfacial water molecules are well ordered and yield spectroscopic features similar to those of the ice–quartz interface. At intermediate pHs the surface water is expected to be less ordered (Du et al., 1994; Ostroverkhov et al., 2004).

Minerals in geochemical environments often have particle sizes as small as few nanometers and expose several surfaces simultaneously, possibly with non-stoichiometric surface compositions (Trainor et al., 2004). Surface defects, absorbents including inorganic and organic ions and molecules, and solution chemistry can complicate the interfacial interactions. The involvement of microbes adds one more level complexity. In most geochemical systems, however, water is the ubiquitous solvent and also participates directly or indirectly in the interfacial chemical reactions. In order to adequately understand and ultimately predict the effects of interaction of aqueous solutions with rocks, sediments, soils, and other natural and synthetic materials, a detailed knowledge of the structure and properties of interfacial water is prerequisite and essential (Thiel and Madey, 1987; Hochella and White, 1990; Brown et al., 1999; Brown, 2001; Henderson, 2002).

The effects of mineral surface structure and composition on the structure and dynamics of the near-surface aqueous fluids are, however, difficult to study and incompletely understood. In addition to the natural complexity of near-surface fluids discussed above, the aqueous phase is statically and dynamically disordered, and there are fewer applicable experimental techniques to probe its properties in situ than are available for probing mineral surfaces (Du et al., 1994; Williams et al., 1998; Teschke et al., 2000; Cheng et al., 2001; Fenter and Sturchio, 2004; Ostroverkhov et al., 2004, 2005; Ruan et al., 2004). It is, thus, instructive to first attempt to understand somewhat idealized systems, starting with the interaction of pure liquid water with perfect mineral surfaces without considering, for instance, chemical reactivity. Molecular computer simulations are extremely efficient in obtaining detailed fundamental information about the behavior of such well-defined systems on the molecular time- and length-scales (e.g., Cygan, 2001). Such insight into the structure of interfacial water is essential to improved understanding of surface-specific experimental data obtained by, for instance, X-ray reflectivity (Cheng et al., 2001), X-ray crystal truncation rod diffraction experiments (Trainor et al., 2004), and sum-frequency vibrational spectroscopy (Ostroverkhov et al., 2004, 2005).

It has long been known that different surfaces affect the structure, dynamical behavior and physical and chemical properties of interfacial water in different ways (Packer, 1977; Beaglehole and Christenson, 1992; Du et al., 1994; Lee and Rossky, 1994; Israelachvili and Wennerström, 1996; Akiyama and Hirata, 1998; Yeganeh et al., 1999; Joseph et al., 2000; Brown, 2001; Scatena et al., 2001; Michot et al., 2002). Computational studies of different oxide and hydroxide surfaces show quite different near-surface water structures and suggest that different surface functional groups can play different roles in developing the interfacial hydrogen bonding networks that are key to understanding near-surface water structure (e.g., Lee and Rossky, 1994; Rustad et al., 2003; Wang et al., 2004b). For instance, molecular modeling shows that the interfacial water molecules at the magnetite (0 0 1) surface accept and donate H-bonds from and to several different surface functional groups (Rustad et al., 2003). For water at the portlandite or brucite (0 0 1) surfaces, MD models show that $Ca_3{}^{VI}OH$ or $Mg_3{}^{VI}OH$ surface functional groups serve as both H-bond donors and acceptors (Kalinichev and Kirkpatrick, 2002; Wang et al., 2004b). For water at a hydroxylated silica surface, simulation results show that interfacial water molecules have two different preferred orientations with different H-bonding configurations (Lee and Rossky, 1994). Detailed and systematic investigation of these issues are essential to further advance our understanding of the ways in which the competing molecular-scale phenomena control the structural and dynamic properties of interfacial water.

In this paper, we present a molecular dynamics (MD) computer simulation study of the interaction of liquid water with the ideal (0 0 1) surfaces of brucite, gibbsite, hydrotalcite, muscovite, and talc. The study is designed to clarify the fundamental molecular-scale relationships between the substrate mineral structure and composition and the structural, transport, and thermodynamic properties of water on these mineral surfaces. These five minerals have different structures, compositions and structural charges and were specifically chosen based on the following criteria. (1) They are representative of important types of mineral surfaces. (2) They have relatively simple and well-known chemical compositions and crystal structures, making the construction of the representative computational MD models tractable. (3) Their surfaces differ from each other in one or more important aspects, including bulk crystal structure, unit cell dimension, permanent structural charge, and hydrophobicity. Common mineral surfaces such as silica and Fe-oxide and hydroxide surfaces were not included, because there has been significant previous computational modeling work on them (e.g., Lee and Rossky, 1994; Spohr et al., 1999; Rustad, 2001; Rustad et al., 2003; Gallo et al., 2002) and because Fe is difficult to model effectively using our force field. Wherever possible, comparisons are made to this previous work. The results of our simulations show that substrate composition, structure and net charge directly affect the structure, H-bonding, hydration energy, and diffusion rates of the interfacial water, with differences in the H-bonding between the substrate and the water playing a key role.

2. Methods

2.1. Substrate mineral structures

Brucite, $Mg(OH)_2$, has a layered structure consisting of single sheets of charge-neutral $Mg(OH)_6$ octahedra, which are stacked parallel to (0 0 1) (Fig. 1A). The brucite structure used as the basis for the surface simulations here (trigonal, $P\bar{3}m1$) is based on neutron diffraction data (Desgranges et al., 1996). The (0 0 1) surface is assumed to expose only OH sites, which are oriented perpendicular to (0 0 1) in the crystal on average (Desgranges et al., 1996).

Gibbsite, $Al(OH)_3$, has a structure similar to brucite, but with only 2/3 of the octahedral sites occupied by Al. There

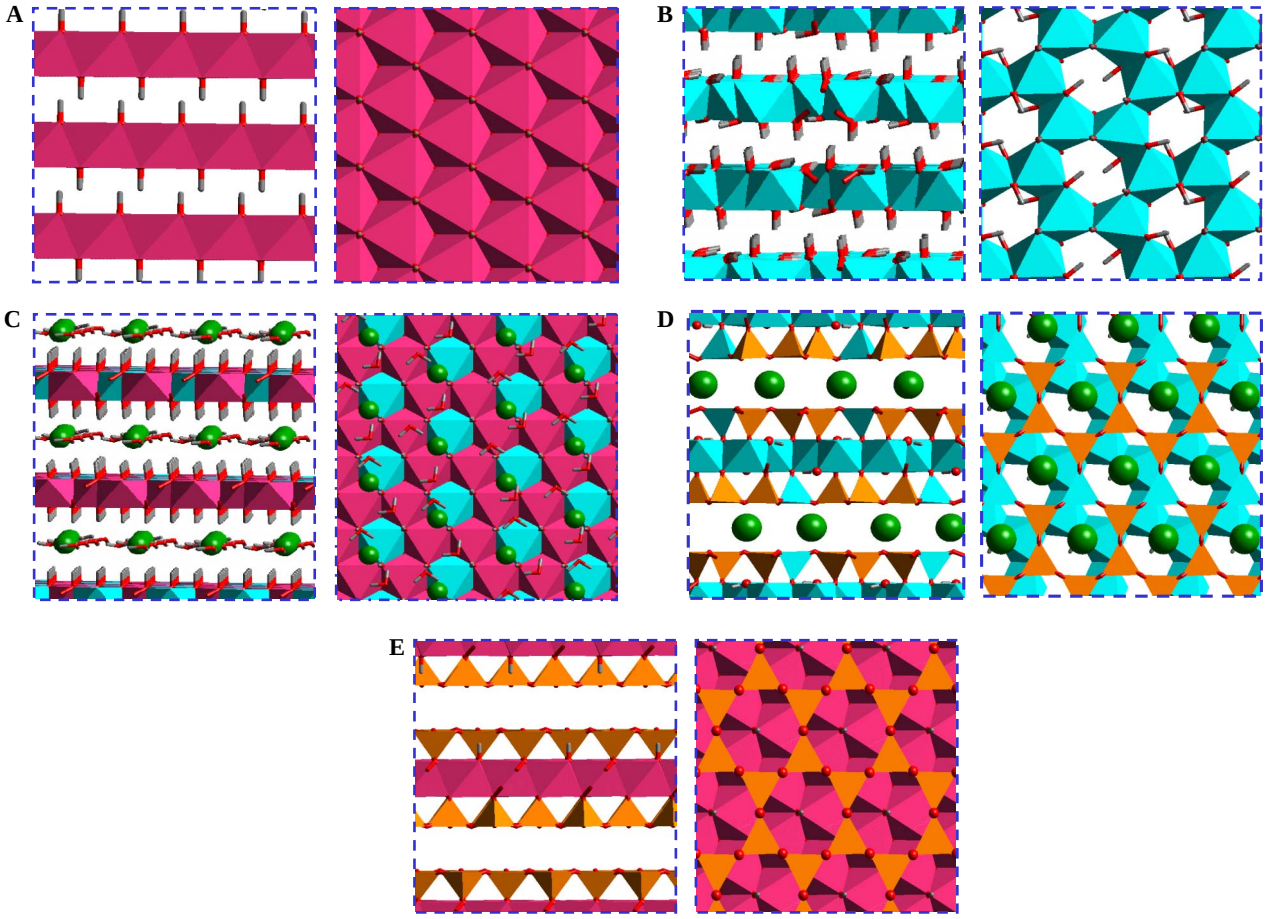

Fig. 1. Different views of the base crystal structures investigated. The figures on the left are parallel to the structural layers and those on the right along the [0 0 1] direction. (A) Brucite, (B) gibbsite, (C) hydrotalcite, (D) muscovite, and (E) talc. The dark/light sticks are OH groups. The cation polyhedra in (A–C) are octahedral sites with the lighter (light blue) ones representing Al octahedra and the darker (pink) ones Mg octahedra. The balls (green) are interlayer Cl^- ions in (C) and interlayer K^+ ions in (D). The triangular shaped polyhedra in (D) and (E) are Si and/or Al tetrahedra. Small balls (red) are oxygen atoms.

are six crystallographically different OH groups, three oriented parallel to (0 0 1) and three perpendicular to it (Saalfeld and Wedde, 1974; Wang and Johnston, 2000, Fig. 1B). The crystal structure used as a basis for the simulations presented here (monoclinic, $P2_1/n$) is based on single crystal X-ray diffraction data (Saalfeld and Wedde, 1974). In both brucite and gibbsite, the octahedral sheets are held together by H-bonding (Wang and Johnston, 2000).

Hydrotalcite, ideally $Mg_2Al(OH)_6Cl \cdot 2H_2O$, is a common layered double hydroxide (LDH). Its structure is similar to that of brucite, except that Al^{3+} for Mg^{2+} substitution causes permanent positive charge development in the trioctahedral hydroxide sheet. This charge is balanced by interlayer anions (here Cl^-), which are normally accompanied by water molecules (Fig. 1C). There are two common polytypes of hydrotalcite-like LDH phases, 3R and 2H (Bellotto et al., 1996). These polytypes have similar local structural environments, but the stacking of their hydroxide layers is different. The Mg/Al hydrotalcite structure used as a basis for our simulations was refined in a rhombohedral unit cell with space group $R\bar{3}m$ (Bellotto et al., 1996; Vucelic et al., 1997). Our models are built assuming $R\bar{3}m$ symmetry for the initial configuration of the primary layers and complete Mg/Al octahedral ordering. Although long-range cation ordering in LDHs has been difficult to observe by powder X-ray diffraction, except for the Ca/Al, Li/Al, and Mg/Ga phases (Terzis et al., 1987; Bellotto et al., 1996), significant short-range cation ordering in them is supported by X-ray absorption spectroscopy (XAS) and nanoscale imaging of molecular sorption onto their surfaces (Cai et al., 1994; Vucelic et al., 1997; Yao et al., 1998). Based on the X-ray powder diffraction structural refinement data (Bellotto et al., 1996), the OH groups at the (0 0 1) surface are, on average, oriented perpendicular to this surface.

At all three of the hydroxide (0 0 1) surfaces investigated here, the surface OH groups form a close packed rhombic lattice, and all three are hydrophilic. The distances between the closest neighboring OH groups are about 3.2, 2.9, and 3.2 Å for the brucite, gibbsite, and hydrotalcite surfaces, respectively. These OH groups have the potential to donate H-bonds to surface water molecules and also to accept H-bonds from these molecules. Thus, different H-bonding configurations with surface OH groups can greatly affect the near-surface water structure and dynamics (Lee and Rossky, 1994; Bridgeman and Skipper, 1997; Spohr et al., 1999; Kalinichev and Kirkpatrick, 2002; Gallo et al., 2002; Wang et al., 2004b). In our computational models for these phases, all OH groups remain intact (i.e., are non-dissociative), and this degree of surface protonation represents thermodynamic states very close to the points of zero net proton charge (pH_{pznpc}). It is known, for instance, that for the gibbsite (0 0 1) surface more than 95% of surface species are $Al_2{}^{VI}OH$ at $pH_{pznpc} \sim 9.0$ (Rosenqvist et al., 2002).

Muscovite, $KAl_2(Si_3Al)O_{10}(OH)_2$, is a sheet-structure alumino-silicate, and the $2M_1$ polytype has monoclinic, $C2/c$ symmetry. The so-called TOT alumino-silicate layers consist of two (Si_3Al) tetrahedral sheets that are held together by a dioctahedral sheet with 2/3 of the octahedral sites occupied by Al. 75% of the tetrahedral sites are occupied by Si and 25% by Al, yielding a structural charge of $-1|e|$ per formula unit (Güven, 1971; Kuwahara, 1999; McKeown et al., 1999). The long-range distribution of Si and Al over the tetrahedral sites is disordered (Brigatti and Guggenheim, 2002), but the short range ordering follows at least the Loewenstein Al-avoidance rule, with no tetrahedral Al–O–Al linkages (Loewenstein, 1954). The negative layer charge is compensated by interlayer K^+ ions, which hold together the TOT layers (Fig. 1D). In our muscovite model, the tetrahedral Al sites are arranged in an ordered fashion such that half of the six-member rings have a Si_4Al_2 composition, the other half have Si_5Al_1, and no tetrahedral Al–O–Al bonds are present. This arrangement mimics a uniform distribution of charge in the tetrahedral sheet as closely as possible in a MD model of limited size, but does impose significant intermediate range order. It is possible that the ordering imposed by this arrangement on the near-surface water molecules in our models is somewhat greater than at real muscovite surfaces. To ensure a uniform structural charge distribution in the crystal structure, all interlayer K^+ were located between one Si_4Al_2 six-member ring and one Si_5Al_1 six-member ring of the opposite TOT layer. The OH groups of the octahedral sheet are oriented almost parallel to the sheets and point towards the vacant octahedral site, in agreement with the experimentally observed orientation (Beran, 2002).

Talc, $Mg_3Si_4O_{10}(OH)_2$, is a silicate with triclinic, $C\bar{1}$, symmetry (Rayner and Brown, 1973). Its crystal structure is similar to that of muscovite, except that all tetrahedral sites are occupied by Si, and the octahedral sheet is trioctahedral and composed of $[MgO_4(OH)_2]$ octahedra. The TOT layer is, thus, electrostatically neutral. The OH groups of the octahedra are oriented perpendicular to (0 0 1) (Rayner and Brown, 1973; Fig. 1E).

2.2. Molecular models of liquid water and mineral–water interfaces

The structure of bulk liquid water, which is the reference state for near-surface water structure studied here, is dominated by distorted tetrahedral local molecular arrangements similar to those in the crystal structure of ice Ih (e.g., Eisenberg and Kauzmann, 1969; Soper, 2000; Errington and Debenedetti, 2001; Head-Gordon and Hura, 2002). In ice Ih, each water molecule has exactly four nearest neighbors. Due to their mutual orientations these molecules are able to donate two H-bonds and accept two others. In liquid water, the long range ice-like molecular ordering is lost, but the local tetrahedral H-bonding arrangement around each individual water molecule is only partially broken. In the bulk liquid phase, the local structural units of distorted H_2O tetrahedra compose an interconnected H-bonding network in which most H_2O

molecules still have four nearest neighbors. Numerous infrared, X-ray and neutron scattering experiments and computational studies provide a quite consistent picture of the local structure of water at ambient conditions (e.g., Eisenberg and Kauzmann, 1969; Robinson et al., 1996; Soper, 2000; Head-Gordon and Hura, 2002). Most of the molecular models of water–water interactions are capable of reproducing these structural features of liquid water (e.g., Jorgensen et al., 1983; Robinson et al., 1996; Wallqvist and Mountain, 1999; Guillot, 2002).

In the SPC (simple point charge) water model used in our simulations, every water molecule has three charged sites centered on each of the H_2O atoms (Berendsen et al., 1981). In addition to the electrostatic interactions between molecules due to these charges, oxygen atoms in this model also interact via a Lennard-Jones potential that emulates the strong repulsion between molecular "cores" at very short intermolecular distances and the weak dispersive attraction at larger distances. The atomic charges and the Lennard-Jones parameters of the SPC water model were specifically optimized to reproduce not only the thermodynamic properties of bulk liquid water at ambient conditions, such as density, energy of vaporization, and heat capacity, but also to reproduce the structure of liquid water in terms of atom–atom radial distribution functions, which are experimentally known from X-ray and neutron diffraction measurements (Berendsen et al., 1981). Over the past two decades, this water model has been thoroughly tested against various experimental data in numerous molecular simulations of aqueous systems (e.g., Jorgensen et al., 1983; Robinson et al., 1996), and despite its relative simplicity has proven to be one of the most reliable. For comprehensive comparisons between various existing models of water–water interaction see the many excellent recent reviews on the subject (Wallqvist and Mountain, 1999; Finney, 2001; Floris and Tani, 1999; Guillot, 2002; Jorgensen and Tirado-Rives, 2005). The SPC water model is incorporated into the recently developed *CLAYFF* force field (Cygan et al., 2004a), which was used for all mineral–water interfacial simulations described here. The simulations were performed at ambient conditions ($T = 300$ K; $P = 0.1$ MPa) and used the Cerius2-4.5 software package (Accelrys, 2000), and previously described MD simulation procedures (Kalinichev et al., 2000; Cygan, 2001; Wang et al., 2001, 2003, 2004b, 2005b; Kalinichev and Kirkpatrick, 2002; Kirkpatrick et al., 2005a,b). Prior to modeling water adsorption on the selected mineral surfaces, MD simulations at constant temperature and pressure (statistical–mechanical *NPT*-ensemble) were carried out to test the performance of our methods and models with respect to the bulk crystal structures of the minerals. These simulations reproduce the experimentally determined bulk crystal structures very well, yielding unit cell dimensions within 5% (and most within 1%) of the experimental values in all dimensions (a, b, c and α, β, γ) except the β value of talc (Table 1). The brucite and gibbsite structures were among those used to empirically parameterize the *CLAYFF* force

Table 1
Summary of cell parameters derived from molecular dynamics simulations of brucite, gibbsite, hydrotalcite, talc, and muscovite

	Brucite $Mg(OH)_2$			Gibbsite $Al(OH)_3$			Hydrotalcite $Mg_2Al(OH)_6Cl{\cdot}2H_2O$			Talc $Mg_3Si_4O_{10}(OH)_2$			Muscovite $KAl_2(Si_3Al)O_{10}(OH)_2$		
	Simulation	Observed[a]	Error (%)	Simulation	Observed[b]	Error (%)	Simulation	Observed[c]	Error (%)	Simulation	Observed[e]	Error (%)	Simulation	Observed[f]	Error (%)
a (Å)	3.152 ± 0.013	3.148(1)	+0.1	8.889 ± 0.019	8.684(1)	+2.4	3.196 ± 0.008	3.0460(1)	+4.9	5.288 ± 0.013	5.293(2)	−0.1	5.183 ± 0.012	5.202(2)	−0.4
b (Å)	3.152 ± 0.013	3.148(1)	+0.1	5.089 ± 0.024	5.078(1)	+0.2	3.197 ± 0.009	3.0460(1)	+4.9	9.155 ± 0.033	9.179(3)	−0.3	8.968 ± 0.028	9.024(3)	−0.4
c (Å)	4.552 ± 0.024	4.779(2)	−4.8	9.726 ± 0.083	9.736(2)	−0.1	23.918 ± 0.143	23.8[d]	+0.5	9.855 ± 0.091	9.469 (3)	+4.1	19.954 ± 0.079	20.078(8)	−0.6
α (°)	89.85 ± 0.37	90.0	−1.7	89.91 ± 0.41	90.0	−0.1	90.73 ± 0.84	90.0	+0.8	89.55 ± 3.22	90.57(3)	−1.1	90.034 ± 0.093	90.0	+0.0
β (°)	90.12 ± 0.29	90.0	+1.3	98.36 ± 1.05	94.54(1)	+4.1	89.37 ± 0.60	90.0	−0.7	109.59 ± 1.53	98.91(3)	+10.7	95.643 ± 0.092	95.756(6)	−0.1
γ (°)	119.98 ± 0.22	120.0	−0.0	90.01 ± 0.16	90.0	+0.0	119.75 ± 0.48	120.0	−0.2	89.98 ± 0.11	90.03(3)	−0.1	89.924 ± 0.049	90.0	−0.1

[a] Desgranges et al. (1996).
[b] Saalfeld and Wedde (1974).
[c] Bellotto et al. (1996).
[d] Boclair et al. (1999).
[e] Rayner and Brown (1973).
[f] Kuwahara (1999).

field (Cygan et al., 2004a), and accurate reproduction of them is expected. However, hydrotalcite, muscovite, and talc were not part of this set, and the high quality of the results for these phases supports the use of *CLAYFF* in our simulations. The discrepancy between the observed and computed β values of talc is due to the relatively larger shift of adjacent TOT layers in our MD simulations than in the experimentally determined structure. The computed value for the displacement between adjacent TOT layers is about 1.8 Å, approximately 0.2 Å larger than the value of $(-0.11a + 0.16b)$ estimated from X-ray data (Rayner and Brown, 1973). However, the fundamental talc TOT structure is reproduced well. The computed displacement between the two tetrahedral sheets of a single TOT layer is also about 1.8 Å, within the computational error of the experimentally observed $a/3$ displacement (Rayner and Brown, 1973). The talc d-spacing was also well reproduced, $c^*_{exp}/c^*_{calc} = 9.355 \pm 0.003/9.285 \pm 0.086$ Å, within 0.8% of the observed value. Recent publications using the *CLAYFF* force field (Kalinichev and Kirkpatrick, 2002; Wang et al., 2003; Cygan et al., 2004a,b; Wang et al., 2004a,b; Greathouse et al., 2005; Kirkpatrick et al., 2005a,b,c; Wang et al., 2005a,b) provide further background and some benchmarking of the performance of this potential model in various geochemical and materials science applications.

The (0 0 1) surfaces for all our mineral models were constructed by cleaving the bulk layered crystal structures along (0 0 1) in the middle of the interlayers. For brucite and gibbsite, the surface OH groups were kept intact and the structural charge remains zero. For hydrotalcite and muscovite, half of the interlayer ions (Cl^- or K^+) were kept at each surface to maintain local charge neutrality. For talc, the (0 0 1) surfaces are the same as the interlayer surfaces and contain only bridging oxygen atoms.

Periodic boundary conditions were applied to the resulting mineral–water interfaces models in all three dimensions, and the simulation supercells contained volumes representing both the crystal phase and water. For the crystal part, the a, b, and c crystallographic dimensions computed in the initial *NPT*-ensemble MD simulations for each bulk phase were repeated 2–4 times and taken as the x, y, and z dimensions of that sub-volume. To minimize the interaction between the two crystal surfaces that are present in or models due to the imposed periodic boundary conditions, the z-dimensions of the computational supercells were set to 100 Å, resulting in a separation of at least 50 Å between the liquid–vapor interface of the adsorbed water film on one solid surface and the other solid surface. Water molecules were initially placed on one solid surface as a slab of liquid water with a density of $\sim$1.0 g/cm^3 and the same x and y dimensions as the crystal supercell. The fractional water coverage (θ) of the surface is evaluated as the ratio of the total number of water molecules on the surface to the number of surface oxygen atoms in the mineral structure. A coverage of $\theta = 1.0$ is a good approximation of one statistical molecular monolayer of H_2O (Cantrell and Ewing, 2001).

To evaluate the diffusive mobility and minimum energy configurations of K^+ ions on the muscovite (0 0 1) surface, a test simulation was carried out by initially placing all K^+ ions in arbitrary positions approximately 3–5 Å from the basal oxygen plane with water coverage of $\theta = 6.65$. During a 500 ps equilibration run, the K^+ ions all moved quickly to their nearest six-member siloxane rings and did not move from those positions during a subsequent 500 ps equilibrium MD simulation. To more realistically simulate the expected minimum energy configurations in the final simulations, the K^+ ions were distributed above all ditrigonal siloxane rings with a Si_4Al_2 composition, because K^+ interaction with this type of ring produces a lower total energy than similar interaction with Si_5Al_1 six-member rings. This is consistent with the results of ab initio calculations (Odelius et al., 1997). Similar preliminary MD simulations for Cl^- on the hydrotalcite (0 0 1) surface showed that in this case Cl^- ions are much more mobile than K^+ on the muscovite surface. In addition, there is noticeable Cl^- exchange among the LDH surface sites and between inner-sphere and outer-sphere coordination environments with characteristic residence times of tens of picoseconds (see also Kalinichev et al., 2000; Kalinichev and Kirkpatrick, 2002). Therefore, for the final hydrotalcite simulations, Cl^- ions were initially placed arbitrarily 3–5 Å from the surface oxygen plane and were free to move.

The final simulations to study water–surface interactions consisted of six different models for each mineral surface, with the models differing in surface coverage (θ) from zero to at least six monolayers. The final x and y dimensions, relevant cell angles, and crystal supercell contents are as follows:

Brucite:	18.78 Å × 18.78 Å, $\gamma = 120°$, four octahedral sheets.
Gibbsite:	26.71Å × 20.37Å, $\beta = 94.54°$, four octahedral sheets.
Hydrotalcite:	19.176 Å × 19.182 Å, $\gamma = 120°$, six octahedral sheets.
Muscovite:	17.79353 Å × 20.7320 Å, rectangular supercell, two TOT layers.
Talc:	21.1403 Å × 18.3175 Å, $\beta = 100°$, two TOT layers.

2.3. MD simulations

All MD simulations for these models were performed using three-dimensional periodic boundary conditions and standard methods and algorithms (e.g., Allen and Tildesley, 1987). Most energy expressions and interatomic interaction parameters were taken directly from *CLAYFF* (Cygan et al., 2004a). Since the partial charges on the oxygen atoms of OH groups and the apical oxygen atoms of the tetrahedra of clay-like sheet-structure alumino-silicates

were originally designed to be compatible with those of brucite, gibbsite, kaolinite, and pyrophyllite, the partial charges for the oxygen atoms of hydrotalcite OH groups and the apical oxygen atoms of the tetrahedra of talc were modified to make the respective computational models electrostatically neutral ($-0.9742|e|$ vs $-0.9500|e|$ in the original *CLAYFF* for hydrotalcite and $-1.2825|e|$ vs $-1.2996|e|$ in the original *CLAYFF* for talc). These small modifications of partial atomic charges (less than 3%) are consistent with the charge-balancing approach in *CLAYFF* (Cygan et al., 2004a) and are expected to not have significant qualitative effect on the simulation results.

The model mineral–water systems constructed as described above were taken as the initial configurations for the MD simulations. The structural relaxation of the models, including all supercell parameters and atom positions, was achieved in four stages (Wang et al., 2003; Wang et al., 2004b). First, the positions of all atoms in the crystalline substrate were fixed, and only the positions and orientations of H_2O molecules and surface ions were allowed to relax in an energy minimization procedure. This was followed by a relatively short (10–50 ps) *NVT*-ensemble MD run. Then the atoms in the substrate were also released, and the energy minimization and MD steps were repeated with all atoms free to relax.

These optimized structures were then used as the starting configurations for the final MD simulations, which were all performed in the *NVT*-ensemble. The constant volume simulations were used to simplify further structural analysis of the adsorbed water films. The constant-volume approach with a fixed cell shape does not introduce significant limitations on the resulting interfacial structure, dynamics and energetics of water, because all the atoms are free to move. A time step of 1.0 fs was used in all cases and each system was allowed to equilibrate for 500 ps of MD simulation. The equilibrium dynamic trajectory for each model was finally recorded for statistical analysis at 10 fs intervals during an additional 500 ps of MD simulation.

2.4. Simulation analysis

Structural analysis of the near-surface water films was undertaken using atomic density profiles in the direction perpendicular to the solid surface, atomic density maps for each atom type within defined slices of the film parallel to the surface (Kalinichev and Kirkpatrick, 2002; Wang et al., 2003, 2004a,b, 2005a,b), and similar profiles and maps for the parameters describing H_2O molecular orientation. These properties were all calculated by averaging over the last 500 ps equilibrium MD trajectory of each system. The position of the mineral surface ($z = 0$) is defined by the average position of the surface oxygen atoms, which belong to surface OH groups for the hydroxides and to surface bridging oxygens for the silicates. The molecular H_2O orientation parameters, φ_D, φ_{HH}, and φ_N, are defined for each water molecule by the angles between the surface normal direction [0 0 1] and the three vectors defining the H_2O orientation. These are, respectively, the dipole vector ($\mathbf{v}_D$), the H–H vector ($\mathbf{v}_{HH}$) from one hydrogen atom to the other, and the normal ($\mathbf{v}_N$) to the H–O–H plane. The positive direction of the surface normal is defined from the substrate to the aqueous phase, and the direction of the H–O–H dipole is from the oxygen atom to the center point between the two hydrogen atoms. The time-averaged statistical distributions of these three angles were calculated as functions of distance from the surfaces.

The diffusion coefficient of water was calculated from the mean square displacement of the oxygen atoms of H_2O:

$$D = \langle |\mathbf{r}(t) - \mathbf{r}(0)|^2 \rangle / 6Nt, \quad (1)$$

where N is the number of atoms, $\mathbf{r}$ is the position of the atom, t is the time, and angular brackets denote the time-averaging along the dynamic trajectory of the system and over all H_2O molecules present. Statistical errors of these calculations are estimated to be within 10–15%. The total diffusion coefficient was calculated in the same way as for a homogeneous bulk system. The water volumes in our systems, however, are not isotropic in all dimensions, and thus we also analyze separately the z and x,y components of the spatial diffusion tensor.

The energy of surface water adsorption (surface hydration), $U_H(N)$, is calculated as

$$\triangle U_H(N) = [\langle U(N) \rangle - \langle U(0) \rangle]/N, \quad (2)$$

where N is the number of water molecules, $\langle U(N) \rangle$ is the average potential energy of an equilibrium system with N water molecules on the surface, and $\langle U(0) \rangle$ is the average potential energy of an equilibrated dry surface (e.g., Smith, 1998). The hydration energy calculated in this way is a convenient and useful parameter to describe the energetics of adsorbed water layers. For comparison with experimentally measured enthalpies of hydration, the $P\Delta V$ term can be safely neglected because $P\Delta V$ is small at ambient pressures. In addition, Whitley and Smith (2004) in their grand-canonical Monte Carlo simulations of montmorillonite clays have recently demonstrated that entropic effects likewise play only a relatively small, compensating role in the total balance of the hydration free energy for such layered mineral structures. Therefore, the hydration energy calculated according to Eq. (2) can be considered a good estimate of the free energy of water adsorption and the relative thermodynamic stability of the hydrated state.

3. Results and discussion

3.1. Hydroxide and sheet silicate (001) surface structures

For the three hydroxide phases studied here, the differences in the structural charge on the octahedral sheet, cation occupancies and distributions, and the orientations of OH groups lead to quite different surface structures. For brucite, the atomic density of an individual surface H_{OH} atom has a triangular distribution with the maxima directly

above the surface O_{OH} atoms (perpendicular to the surface; Fig. 2A). The triangular distribution is due to a small but significant probability of the OH group being tilted with equal probability towards the three neighboring tetrahedral vacancies on the surface. This orientation slightly decreases the electrostatic repulsion between positively charged H_{OH} and Mg atoms, and is qualitatively similar to the "three-site split-atom" model of Desgranges et al. (1996) for the positions of H_{OH} atoms in bulk brucite. In this model, the hydrogens are statistically split among three equally occupied sites, and the O–H direction is tilted toward the nearest O_{OH} in the other octahedral layer, making an angle with the threefold axis of about 9° at room temperature. The surface relaxation at the brucite (001) surface is very limited and is within the error of our MD calculations. This is consistent with ab initio calculation for this surface that shows less than 0.01 Å relaxation relative to the ideal termination of the bulk crystal (Masini and Bernasconi, 2002). This happens because cleavage of this surface occurs through relatively weak H-bonds between adjacent octahedral hydroxide sheets, and adsorbed H_2O molecules on the surface do not have a strong effect on its structure.

For the gibbsite surface (Fig. 2B), there are two orientations for surface OH groups, because only 2/3 of the octahedral sites are occupied by Al and 1/3 are vacant. Thus, 1/3 of the surface OH groups are tilted slightly towards the octahedral vacancies at an angle of about 15° with the surface normal. The other 2/3 of OH groups are dynamically distributed between two preferred orientations. Statistically, about 25% of the time these OH groups are nearly perpendicular to the surface and 75% of the time they point toward the octahedral vacancies and are oriented about 90° to the surface normal, almost parallel to the (001) surface (Fig. 2B). This picture is similar to the OH orientations in bulk gibbsite determined by single crystal X-ray refinement (Saalfeld and Wedde, 1974), in which half of the OH groups are parallel to (001) and the other half are perpendicular to it (Saalfeld and Wedde, 1974; Wang and Johnston, 2000). Our MD simulations of bulk gibbsite yield the same picture. As for brucite, surface relaxation at the gibbsite (001) surface is very limited and for the same reasons.

For the hydrotalcite (001) surface, the H_{OH} distribution shows a maximum directly above O_{OH}, resulting in an OH orientation perpendicular to the surface, even though each OH group is coordinated to two Mg and one Al. (Fig. 2C). The electrostatic field of the positively charged octahedral sheet is the dominant cause of this alignment. The surface Cl^- ions are dynamically distributed across the surface and also contribute to the orientation of the surface OH groups.

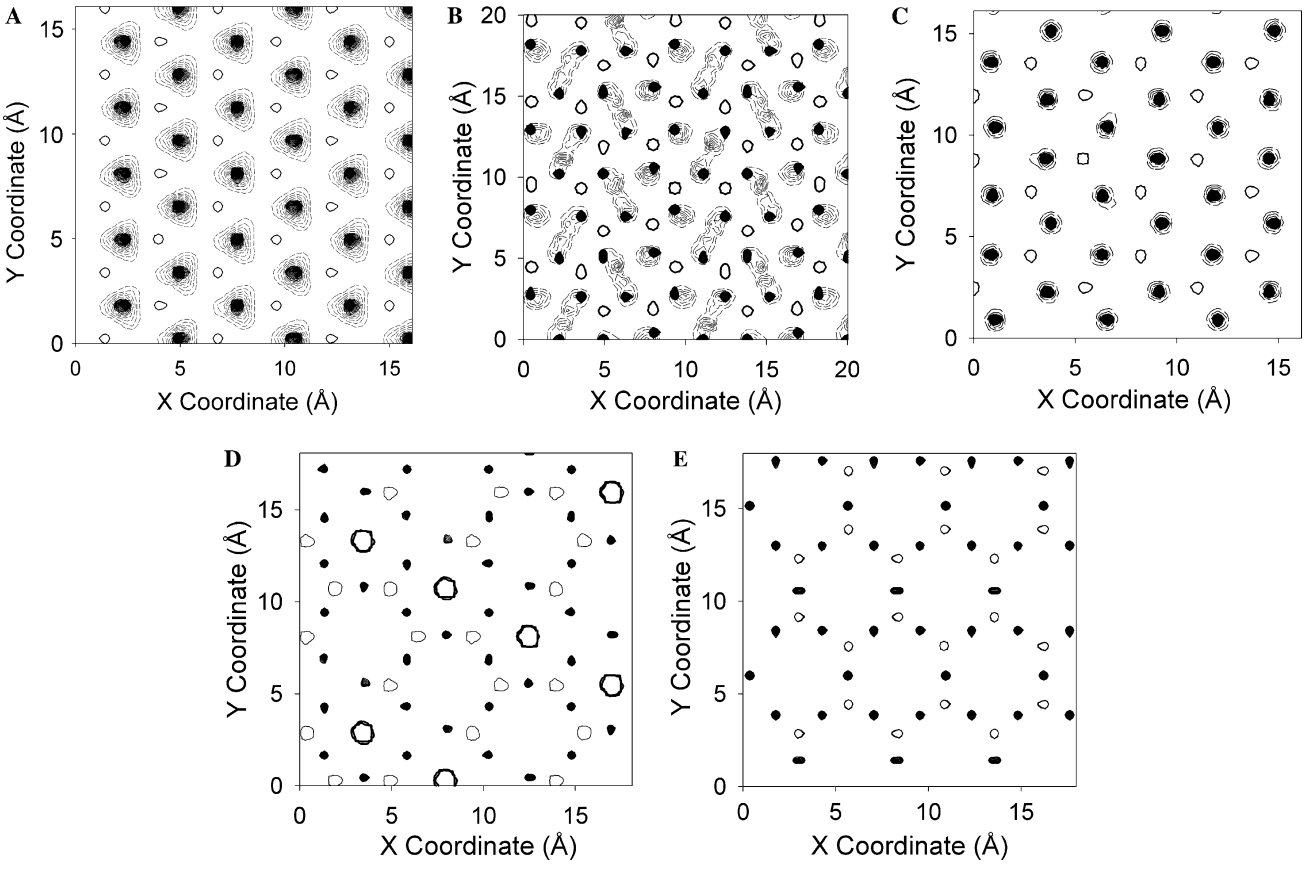

Fig. 2. Atomic density contour maps of the substrate mineral surfaces. The black dots are surface oxygen atoms. The thin dashed contours are hydrogen atoms of surface OH groups. The open small circles are the cations in the polyhedra. The missing cation positions in (C) are Al in octahedral, in (D) are Al in tetrahedra. Large circles in (D) are surface K ions.

For muscovite and talc (Figs. 2D and E), the surface oxygen atoms do not form a closely packed array but rather reflect the structure of the siloxane tetrahedral sheet. On muscovite, K^+ ions are located directly above the vacancies at the centers of the six-member rings of tetrahedra and are coordinated by six surface bridging oxygens. These K^+ ions do not migrate from their positions over the 500 ps time scale of our MD simulations. The OH groups of the octahedral sheet are parallel to (001). Overall, the computed (001) surface of muscovite is very similar to the siloxane interlayer surface in the bulk crystal (Güven, 1971; Kuwahara, 1999; McKeown et al., 1999), as suggested by experimental AFM study in fluid contact mode (Kuwahara, 1999). Similarly, the computed talc surface closely resembles the siloxane layer in bulk talc. The OH groups of the octahedral sheet are perpendicular to (001). The surface relaxation for the muscovite (001) surface is larger than for the hydroxides. The distance from K^+ to the surface bridging oxygen atoms is about 0.1 Å less than that in the bulk. This result is qualitatively consistent with X-ray reflectivity measurements that indicate that the outermost polyhedral layer has an inward displacement of 0.04 Å (Cheng et al., 2001).

3.2. Atomic density profiles of adsorbed water

The density profiles of adsorbed H_2O molecules are significantly different for different substrates and provide the basis for understanding how these surfaces perturb the structure of the interfacial water (Fig. 3). The center of mass of a water molecule is almost coincident with the center of its oxygen atom, and thus the O_{H_2O} density profile effectively represents the molecular density distribution of interfacial water. The density maxima in the profiles for the three hydroxide surfaces have very similar positions, intensities, and shapes, and in all three cases detectable surface effects extend to about 10 Å from the surface. The first density maxima are located at 2.40, 2.55, and 2.57 Å from the surfaces of brucite, gibbsite and hydrotalcite, respectively, the second maxima are at 4.95, 5.10, and 4.90 Å, and the third maxima are at 6.30, 6.50, and 6.90 Å. Broad peaks between 8 and 10 Å are also present for all three. MD-simulated atomic density profiles of water on the portlandite, $Ca(OH)_2$, (001) surface also have similar characteristics (Kalinichev and Kirkpatrick, 2002). The similarities in these density profiles are due principally to the similar rhombic arrays of OH groups on these surfaces, and in large part they are independent of net structural charge and the orientations of the surface OH groups. The small differences in the positions of the maxima for brucite and gibbsite are due to the smaller surface OH–OH distance for gibbsite. For portlandite, which has a larger OH–OH distance, the O_{H_2O} density profile maxima are located at 2.55, 4.75, and 6.45 Å, in agreement with this conclusion.

The O_{H_2O} density profiles at the muscovite and talc (001) surfaces are quite different from each other and also very different from those at the hydroxide surfaces (Fig. 3). The profile for muscovite exhibits more features than that for talc, reflecting significantly greater structuring of the interfacial water by the muscovite surface. For muscovite, there are five density maxima at about 1.7, 2.7, 3.6, 5.4, and 6.3 Å, and a weak, asymmetric and broad peak between 8 and 11 Å. Smaller but statistically meaningful

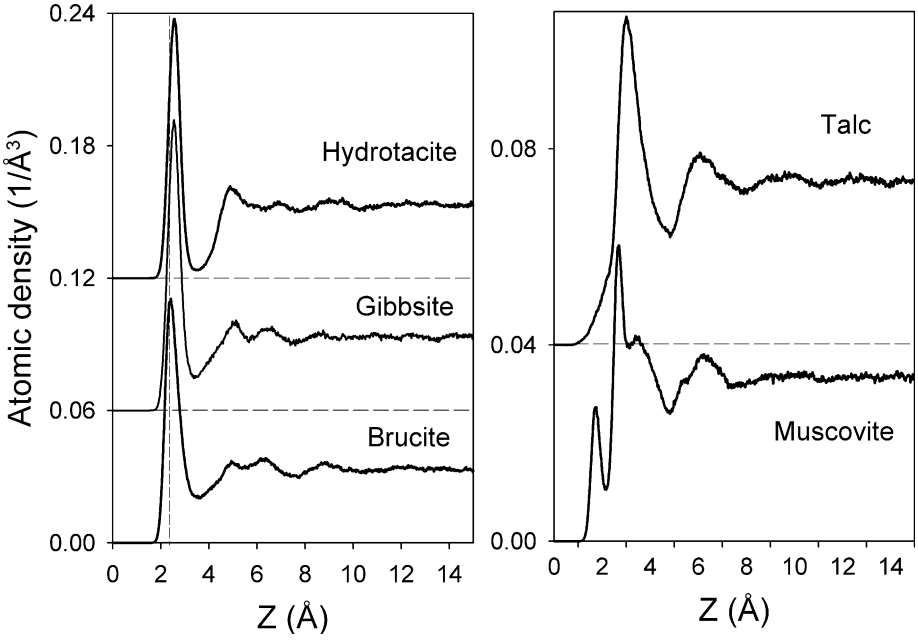

Fig. 3. Atomic density profiles of O_{H_2O} at the modeled (001) surfaces at the largest water coverages. Only results up to 15 Å from the surface are shown, because there is no significant change at larger distances. The origin ($z = 0$) is taken as the average position of the surface oxygen atoms (oxygen atoms of surface OH groups for the three hydroxides and surface bridging oxygens for the sheet silicates).

variations in atomic density extend more than 15 Å from the surface. For talc there are two peaks at about 3.1 and 6.2 Å, and two less pronounced broad peaks from 8 to 11 and from 11 to 14 Å. The latter two peaks are more prominent for talc than for muscovite. Similarities between the density profiles for muscovite and talc include intensity maxima centered at about 1.7, 3.6, and 5.4 Å, although these are somewhat hidden for talc by the maxima at 3.1 and 6.2 Å. In addition, a distinct shoulder at about 1.7 Å in the talc profile corresponds to the first peak in the muscovite profile, in which it is much stronger and clearly distinguishable from the next, more intense peak (about 2.7 Å for muscovite and about 3.1 Å for talc). The molecules contributing to the atomic density near the peak at ~1.7Å are adsorbed in the vacancies at the centers of six-member rings for both phases. Adsorption of water molecules at such sites has been observed previously by neutron diffraction and predicted by computer simulations of the hydrated interlayers of vermiculite (Skipper et al., 1991; Arab et al., 2003), montmorillonite (Karaborni et al., 1996), and muscovite surface (Cheng et al., 2001; Park and Sposito, 2002). Monte Carlo simulation of the water–talc interface has also shown that the first adsorbed molecules are located above the six-member rings (Bridgeman and Skipper, 1997). The peak positions of the O_{H_2O} density profile in this study cannot, however, be compared directly with our results, because the position of surface bridging oxygens is not clearly provided (Bridgeman and Skipper, 1997). Since the muscovite surface has a net negative structural charge, the adsorbed water molecules in the vacancies interact with it more strongly than with talc. The peak at 3.1 Å for the talc–water interface corresponds to the combined 2.7 and 3.6 Å peaks of the muscovite–water interface, and the molecules contributing to these peaks are adsorbed above the surface bridging oxygens in our previous MD simulations (Wang et al., 2005a).

One important difference between the O_{H_2O} density profiles for the talc–water interface and for all other interfaces is that for talc the principal density maxima are all nearly equidistant (approximately 3.1 Å) from each other. The profiles of the other substrates show more complex patterns. The equal spacing between maxima at the talc–water interface clearly reflects the dominance of so-called "excluded volume" or "hard wall" effects (Abraham, 1978; Yu et al., 1999) for this system. These molecular packing effects are geometrical in origin, with the fluid density perpendicular to the surface oscillating with a periodicity equal to the diameter of molecules in the fluid (Abraham, 1978; Yu et al., 1999). They are dominant in relatively simple cases of fluid structuring near solid surfaces, such as a hard sphere fluid at a hard wall or a Lennard-Jones fluid at a Lennard-Jones surface. "Hard wall" surfaces do not normally have specific sites for interaction with water molecules, such as H-bond acceptor and/or donor sites, and because they do not interact strongly with water molecules, they are hydrophobic. The absence of such interactions on a molecular scale is the origin of macroscopic hydrophobic behavior. Similar equal spacings were observed in MD simulations of water density profiles at the liquid mercury surface, where the O_{H_2O} density maxima are also about 3 Å apart (Bopp and Heinzinger, 1998; Dimitrov et al., 2001). The minor deviations from perfect density maximum periodicity at the talc surface, including the asymmetrical shape of the peaks and shoulders, are related to the structural details of the talc (0 0 1) surface. As discussed above, the shoulder at 1.7 Å occurs due to the water molecules occupying the vacancies in the six-member rings on the talc surface, a possibility that does not exist for a perfectly smooth "hard wall" surface.

For the other interfaces studied here, the non-uniform peak spacing of the surface water density profiles reflects the significance of the specific structure of the substrate, its ability to form stable H-bonding between the surface and water molecules, and the propagation of these surface H-bonding effects into the fluid phase. Similar features are observed in molecular simulations of other hydrophilic surfaces where interfacial H-bonding is a significant factor (Karim and Haymet, 1988; McCarthy et al., 1996; Stöckelmann and Hentschke, 1999; Bryk and Haymet, 2002). At the NaCl (0 0 1) surface, the water density maxima are at 2.3, 3.4, and 6.0 Å (Stöckelmann and Hentschke, 1999), and at the MgO (0 0 1) surface, they are at 2.1, 4.6, 6.4, and 8.5 Å (McCarthy et al., 1996).

The close similarities in the O_{H_2O} density profiles for three hydroxide (0 0 1) interfaces and both the similarities and the differences for two sheet silicate (0 0 1) interfaces indicate that both the substrate crystal structure and the surface hydrophobicity play important roles in defining the interfacial water density structure normal to the surface and that substrate structural charge and the presence of charge balancing ions at the surface are less important. Surface crystal structure (geometry and bond lengths) provides a critical geometric constraint ("pattern") for the formation of H-bonds with the interfacial water molecules. This patterning is reflected in the peak positions and spacing of the water density profile. Hydrophobicity is a measure of the strength of H-bonding between the surface and adsorbed water molecules. The more hydrophobic the substrate surface, the fewer constraints it can exert on the interfacial water density profile. The occurrence of the first maximum in the O_{H_2O} density profile for brucite at approximately 2.45 Å from the surface (Fig. 3) results from the contributions of two intermixed groups of water molecules at 2.3 and 2.6 Å from the surface. Those in the nearer group typically donate H-bonds to the surface, whereas those in the further group typically accept H-bonds from it (Wang et al., 2004b). If all the water molecules were located directly above the vacant tetrahedral sites, the O-density maximum would be about 2.1 Å from the surface, assuming a distance of 2.8 Å between O_{OH} and O_{H_2O}, which is the position of the first peak of O–O RDF in bulk water (e.g., Head-Gordon and Hura, 2002), and a distance of 3.1 Å between the nearest neighboring OH groups on the surface, which is

the value in bulk brucite (Wang et al., 2004b). For water at the NaCl (100) surface, the first peak in the O_{H_2O} density profile is at 2.3 Å, which is close to the Na–O_{H_2O} distance in bulk aqueous solution (Stöckelmann and Hentschke, 1999). Water molecules are adsorbed above the Na^+ ions on the surface and H_2O dipoles point away and are unable to form strong H-bonds with it (Stöckelmann and Hentschke, 1999). On the idealized, non-hydroxylated MgO (001) surface, the first peak of the water density profile is at about 2.2 Å, because H_2O molecules can only donate H-bonds to the surface O atoms or participate in H-bonding with other H_2O molecules (McCarthy et al., 1996). For a hydrophobic surface such as talc (001), the details of the surface structure are less important in terms of the peak positions in the O_{H_2O} density compared to a hydrophilic surface such as muscovite (001). Thus, the position of the first peak in the adsorbed water molecular density profile is more substrate-specific if the substrate is hydrophilic.

3.3. Substrate induced ordering in the interfacial plane and water dipole orientations

The atomic density profiles discussed in the previous section provide information about only the structural arrangement normal to the surface and by themselves are not sufficient to develop an adequate picture of the substrate effects on the interfacial water structure. The H_2O atomic density distributions within the plane of the surface and the variation of the H_2O orientations with distance from the surface provide important additional insight (Figs. 4 and 5). As for the density profiles, these structural features are greatly affected by the substrate surface structure, composition and charge.

In all cases studied here, the O_{H_2O} atomic probability density contour maps in the *x–y* plane immediately adjacent the surface are quite ordered and the water molecules have clearly preferred surface sites that reflect the substrate surface structure (Fig. 4). These contour maps were

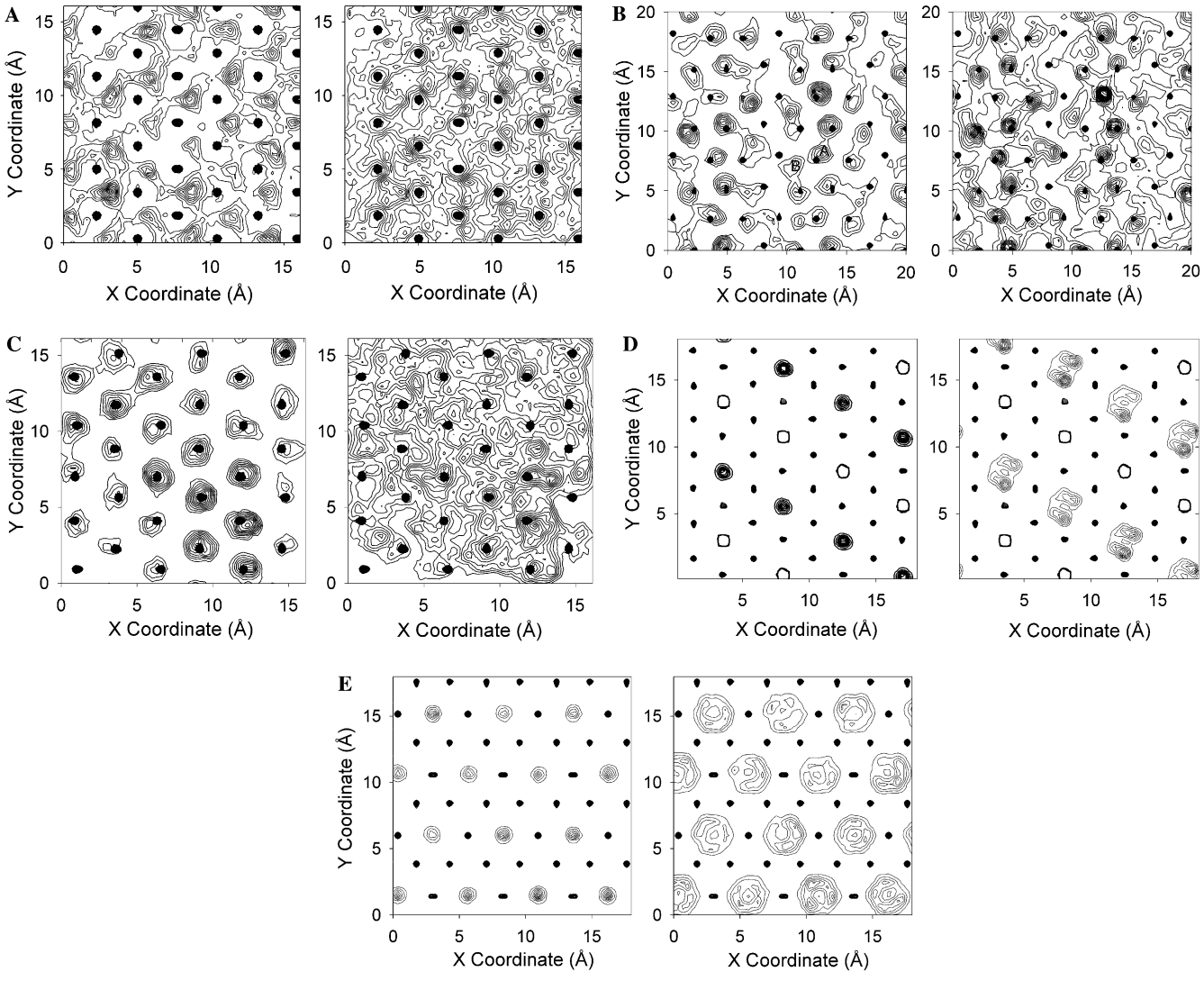

Fig. 4. Atomic density contour maps for the first layer of adsorbed water molecules on the surfaces studied. The black dots are surface oxygen atoms. The figures on the left are for O_{H_2O}, and those on the right are for H_{H_2O}. (A) Brucite, (B) gibbsite, (C) hydrotalcite, (D) muscovite, and (E) talc.

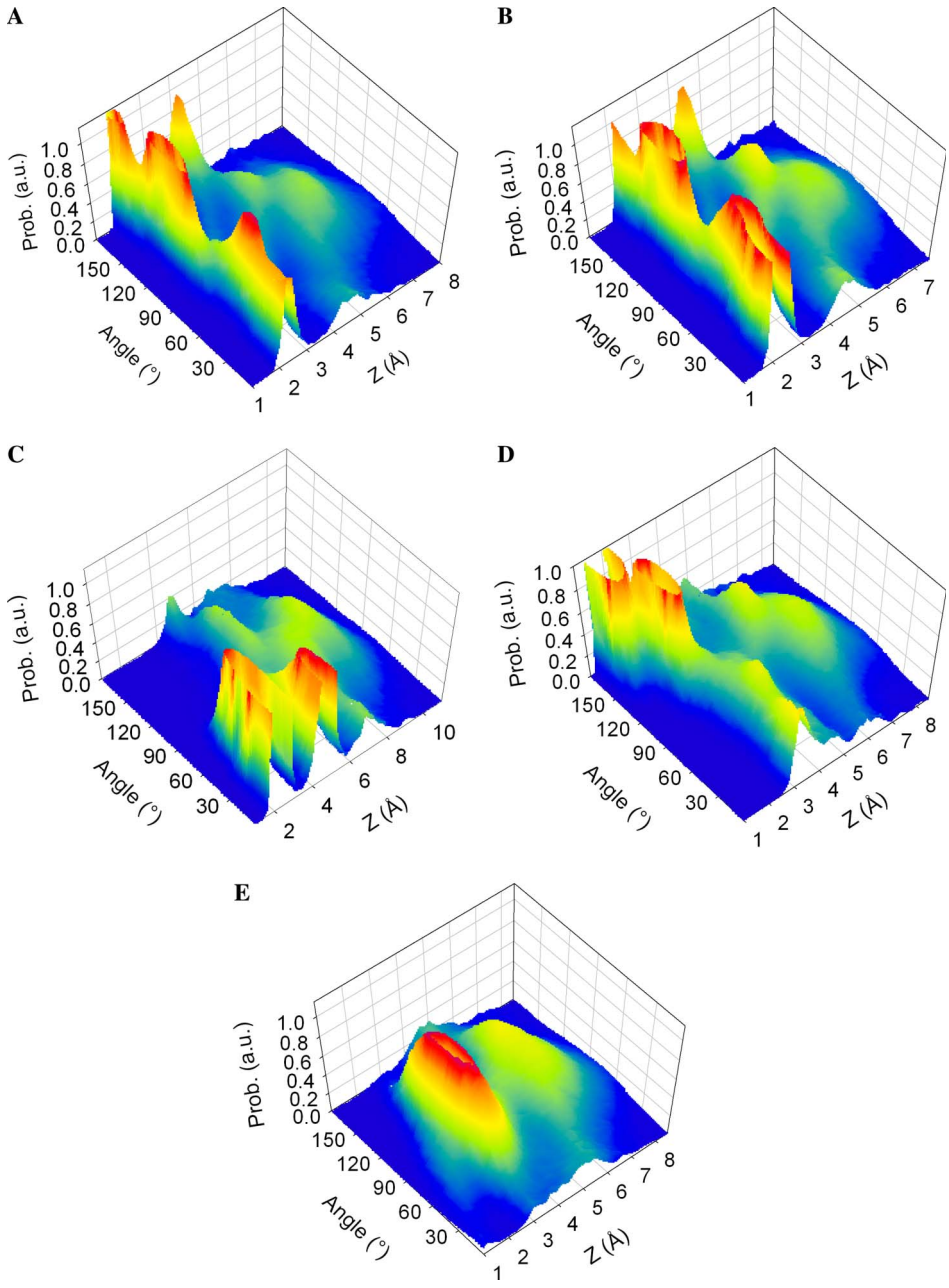

Fig. 5. MD computed relative probability distributions (in arbitrary units) of the angle between the H_2O dipole and the surface normal as a function of distance from the surface for interfacial water molecules. (A) Brucite, (B) gibbsite, (C) hydrotalcite, (D) muscovite, and (E) talc.

calculated for water molecules located at distances contributing to the first peak (the shoulder for talc) in the O_{H_2O} density profiles. For the complicated muscovite surface, this includes all molecules at distances between 1.2 and 2.1 Å from the surface. The probability distributions of the water dipole orientations also show substrate-specific patterns that vary in complex ways with distance from the surfaces (Fig. 5). The dipole orientations in the first few layers of interfacial water are highly ordered, reflecting the surface structure, net structural charge, and surface hydrophobicity.

For brucite, most molecules are preferentially located above the vacant tetrahedral sites of the trioctahedral sheet (Fig. 4A, left), towards which the surface OH groups are tilted (Wang et al., 2004b). These water molecules form a dynamical but reasonably well-ordered two-dimensional hexagonal arrangement with a quasi (1×1) superstructure that reflects the underlying brucite structure. The distribution of the H_{H_2O} atomic density is also quite well ordered (Fig. 4A, right), and there are three noticeable maxima associated with each water adsorption site. These lie on the line between the O_{H_2O} position (above the center of the tetrahedral vacancies) sites and the surface O_{OH}.

For the gibbsite surface, there are two types of O_{H_2O} water adsorption sites that are quite different from those on the brucite surface, but that result in similar preferred

surface H_2O orientations (Figs. 4B and 5B). One of these sites, labeled as "A," is located above and outside the vacant octahedral sites and close to surface O_{OH} sites in which most OH-groups are oriented parallel to the surface. Most of these water molecules are oriented with their dipoles pointing towards the surface and donate H-bonds to surface O_{OH}. The other type of surface water site, labeled as "B," is located directly above the centers of the vacant octahedral sites. Water molecules at most of these sites are oriented with their dipoles pointing away the surface and accept H-bonds from the surface OH groups. The positional distributions in the H_{H_2O} density map are broader but similar to those in the O_{H_2O} density map, and the local density maxima are almost coincident (Fig. 4B, right). The hydroxide (0 0 1) surface of the dioctahedral sheet of kaolinite is very similar to the gibbsite (0 0 1) surface, and ab initio calculations identified only a single site of water adsorption on this surface (Tunega et al., 2002). This is located directly above the octahedral vacancy and the H_2O orientation is similar to our results for such sites.

The water orientation distributions at the brucite and gibbsite surfaces (Figs. 5A and B) are very similar in shape, relative intensity and dependence on distance from the surface. This is because these surfaces have nearly the same rhombic, close packed surface OH arrangements and bear no structural charge. The time-averaged orientation of the surface OH-groups does not seem to significantly affect the time-averaged orientation of these water molecules. Rather, the relative proportions of donating and accepting H-bonds between surface OH-groups and water molecules is more important in influencing the time-averaged molecular orientations, because H-bonding is directional in nature. The molecules contributing to the first peak of the O_{H_2O} density profiles at the brucite and gibbsite surfaces have two different orientations, and individual molecules with these orientations are intimately mixed across the surfaces in the x–y plane (Wang et al., 2004b). Some of them point their dipoles toward the surface and these molecules donate H-bonds to surface OH groups. The others point their dipoles away from the surface, and these molecules accept H-bonds from the surface OH groups. This ability of surface water molecules to both donate H-bonds to and accept H-bonds from the surface OH groups is in agreement with ab initio molecular dynamics simulations of water adsorbed at a hydroxide surface of kaolinite (Tunega et al., 2004).

For hydrotalcite, the O_{H_2O} density map has maxima directly above the surface OH groups (Fig. 4C, left), and the H_{H_2O} map has maxima at the same locations, but their distribution is much more disordered (Fig. 4C, right). The water dipoles are oriented away from the surface, reflecting the strong attractive interaction between the positively charged surface and negative (oxygen) ends of the H_2O molecules. These molecules accept H-bonds from the surface OH groups but do not donate H-bonds to the O_{OH} (Fig. 5C). This H-bonding configuration is very similar to that at the hydrocalumite (0 0 1) surface (Kalinichev and Kirkpatrick, 2002). Hydrocalumite (Friedel's salt) is a Ca/Al LDH, $[Ca_2Al(OH)_6]Cl\cdot 2H_2O$ with a structure similar to but more ordered than hydrotalcite (Terzis et al., 1987). The alignment of the water molecules on the hydrotalcite and hydrocalumite surfaces and the absence of H-bond donation to the surface are due to repulsion by their positively charged substrate structures.

For the muscovite and talc surfaces the adsorption sites nearest to the surface are located above the centers of the vacancies in the six-member siloxane rings (Figs. 4D and E). For talc, these sites are at least partly stabilized by weak H-bonding from the OH groups of the octahedral layers. The H_{OH} maps and water dipole orientations for muscovite and talc are quite different, however, because of the different surface charge (Figs. 4D, E and 5D, E). At the muscovite surface (Fig. 4D), the H_2O molecules have dipoles pointing towards the surface and donate H-bonds to the bridging oxygens (Fig. 5D). The tetrahedral Al for Si substitution causes the negative charge on the bridging oxygens connecting Al and Si (Al–O–Si) to be larger than on Si–O–Si, and these oxygens become preferential acceptors of H-bonds from H_2O. This preference gives rise to the paired H-maxima shown in Fig. 4D (right). In our models, the tetrahedral Si,Al distribution is ordered, whereas in real muscovite it is not. Similar local H-bonding environments should be present, however.

At the talc surface (Fig. 4E), the interfacial water molecules accept weak H-bonds from the OH groups of the octahedral sheet. The six weak H_{H_2O} atomic density maxima indicate that the water molecules also donate weak H-bonds to the surface bridging oxygens. The small number of water molecules closest to the surface (a weak shoulder of the O_{H_2O} density profile at ~1.2–2.1 Å) have their dipoles pointed away from it, allowing them to accept H-bonds from the OH groups of the octahedral sheet (Fig. 5E). However, the majority of the surface water molecules on talc, that is, the ones contributing to the first O_{H_2O} density profile peak between 2.5 and 4.5 Å, have their dipoles more or less parallel to the surface, reflecting the hydrophobic character of talc. This orientation is in good agreement with the results of other molecular dynamics simulations (Arab et al., 2003), quantum chemical DFT calculation (Bridgeman et al., 1996), and Monte Carlo simulations (Bridgeman and Skipper, 1997) for talc (0 0 1) that all show adsorbed water molecules located at the centers of the six-member rings.

In contrast, recent ab initio calculations of single molecule and monolayer water adsorption on the electrostatically neutral tetrahedral (siloxane) kaolinite (0 0 1) surface, analogous to talc (0 0 1), yield predicted water dipole orientations pointing towards the surface (Tunega et al., 2002, 2004). In addition to obvious differences between classical and quantum approaches, another reason for this discrepancy could be that such mono-molecular calculations do not account for changes in the potential energy landscape seen by a water molecule due to the presence of other water molecules near the surface, most

importantly the absence of lateral interaction among water molecules (Tunega et al., 2002). The ab initio MD simulation of monolayer adsorption of the kaolinite tetrahedral surface (Tunega et al., 2004) also shows no noticeable ordering of the adsorbed water molecules. In contrast, both orientational and spatial ordering (but not ice-like ordering) within the near-surface plane of adsorbed water molecules are clearly observable at the talc surface of our MD simulations (Figs. 4E and 5E). The ab initio MD simulation was performed for a duration of only 4 ps. If quantum effects on the structural ordering of the molecularly adsorbed interfacial water are not significant, the short time of the ab initio MD simulation could have contributed to the degree of the molecular disordering, where the molecular structure could be relative stable with respect to its initial state. It is well known that the H-bond life times and H_2O reorientation times in liquid water at ambient conditions are of the order of 2–5 ps (Ohtaki and Radnai, 1993; Luzar, 2000) and can be much longer for water molecules at a solid surface (e.g., Ruan et al., 2004). Thus, the ab initio MD simulation may have been able to probe only a relatively small region of the system's phase space and characterize only the vicinity of one of its local energy minima. If this is the case, the resulting structure would be significantly dependent on the initial configuration of the surface water molecules. In contrast, our equilibrium MD simulations extended for 500 ps after an initial 500 ps equilibration period.

The strong similarities between the structures of the near-surface water and the substrates discussed above are controlled by the substrate surface structure and its ability to form H-bonds with the adsorbed water molecules. For the three hydroxide surfaces studied here, the surface OH structures are very similar, but the abilities of the surfaces to form H-bonds and different H-bonding configurations with water molecules lead to quite different adsorption density maps and dipole orientations. For the hydrotalcite surface, the positive net structural charge of the substrate allows water molecules to only accept H-bonds from the surface OH groups, resulting in the single adsorption site. At the brucite surface, the OH groups are tilted towards vacant surface tetrahedral sites, making the immediate neighborhood of these sites very favorable for the adsorption of water molecules that are oriented to accept H-bonds from the surface OH groups. At the gibbsite surface, however, the OH groups are tilted toward vacant surface octahedral sites, and these sites become strongly preferred for the adsorption of H_2O molecules, which accept H-bonds from the surface OH groups. The other adsorption site for gibbsite is preferred by water molecules oriented to donate H-bonds to these surface OH groups that are oriented almost parallel to the surface. For many (0 0 1) surfaces of sheet silicates, including talc and muscovite, the adsorption sites are invariably the vacancies in the six-member rings, although the H-bonding depends on the surface charge distribution.

Similar close relationships between the substrate surface structure and the structural arrangement of the first layer of water molecules have also been observed for other water–solid interfacial systems and seem quite general. For instance, MD simulations show that the two-dimensional structure of the first layer of water on the NaCl (1 0 0) surface reflects the underlying NaCl crystal structure (Stöckelmann and Hentschke, 1999). The electrostatic attraction between Na^+ and negatively charged O_{H_2O} is stronger than the hydrogen bonds between H_2O and surface Cl^- ions, resulting in the preferred water adsorption site being directly above each surface Na^+ ion, with the water dipole pointing away from the surface (Stöckelmann and Hentschke, 1999). At the liquid mercury interface, H_2O molecules are adsorbed above mercury atoms because of the weak attractive interaction between the water molecules and the mercury atoms (Bopp and Heinzinger, 1998).

Net structural substrate charge plays a dominant role in controlling the H_2O dipole orientation in the first layers of water at all of the surfaces studied here. Positively charged surfaces orient water dipoles to point away from the surface, whereas those with negative structural charges have the opposite effect. Similar effects have been observed in sum-frequency vibrational spectroscopic (SFVS) measurements at the surfaces without permanent structural charge but which develop a surface charge due to pH-dependent protonation/deprotonation surface reactions (Du et al., 1994; Yeganeh et al., 1999; Ostroverkhov et al., 2004, 2005) and in simulations of the application of a permanent electrostatic field to metal–water interfaces (Spohr, 1999). SFVS experiments show that change of solution pH across the iso-electric point of the Al_2O_3 (sapphire) surface causes the interfacial water dipoles to flip 180° (Yeganeh et al., 1999), and similar effects are observed at the quartz surface (Ostroverkhov et al., 2004, 2005). The calculations of Spohr (1999) for metal surfaces show that at a surface charge density of $-9.9\ \mu C/cm^2$ about 80% of the surface water molecules have their dipoles pointing towards the surface, whereas at a surface charge density of $+9.9\ \mu C/cm^2$, about 70% of them point away from the surface. Our results for the electrostatically neutral, hydrophylic hydroxide phases described here and elsewhere (Kalinichev and Kirkpatrick, 2002; Wang et al., 2004b) show that in this case surface water dipoles point both towards and away the surface and that molecules with both orientations are mixed on the molecular scale across the surface.

Compared to bulk liquid water, for which the distributions of atomic density and dipole orientation would be isotropic and flat, the non-uniform distributions for the H_2O molecules near mineral surfaces indicate substantially restricted static and dynamic translational and orientational ordering and thus reduced orientational and translational entropy. The peaks in the molecular density and orientational distributions at hydrophilic surfaces (here hydroxides and muscovite) are narrower than at a hydrophobic surface (here talc), indicating greater ordering of

water at hydrophilic surfaces compared to the hydrophobic ones.

3.4. Diffusion of adsorbed water on mineral surfaces

The computed H_2O self-diffusion coefficients on the modeled surfaces vary significantly with water coverage, and this variation is quite different at the hydrophobic surface of talc than at the other (hydrophilic) surfaces (Fig. 6). For all phases, however, the components of the diffusion coefficient tensors parallel to the surface (*XX* and *YY* components) are much larger than the *ZZ* component perpendicular to it. This is because diffusion perpendicular to the surfaces is greatly restricted by the film thickness (water coverage, θ), and the computed *ZZ* root-mean square displacements must be small, because the molecules cannot move very far in that direction. The *ZZ* diffusion coefficients increase with increasing water coverage at $\theta > 1.0$ and reach a value of about 1.0×10^{-5} cm^2/s at $\theta = 6.0$ at all the surfaces. This greater mobility of H_2O within the surface plane has also been observed in previous MD computations of water in brucite (0 0 1) nano-pores (Sakuma et al., 2003). In that study, the self-diffusion coefficient of near-surface water in the *x*–*y* plane is approximately 1.5 times greater than the computed bulk-liquid value. Our results for brucite do not reproduce values greater then the bulk value, but the observation that diffusion in the *x*–*y* plane is always faster than in the *z* direction suggests that this behavior may be general and independent of the details of surface structure and charge. At the range of water coverages we studied, the surfaces, both mineral–water or vacuum–water, act like a restricting barrier, which limits the mobility of the water molecules perpendicular to the surfaces and increases the mobility within the surface plane.

For the hydrophilic phases, the smallest average diffusion coefficients occur at near monolayer coverages of $\theta \sim 1.0$, and they increase towards the bulk value of ca. 2.8×10^{-5} cm^2/s (Guillot, 2002) with increasing water film thickness (Figs. 6A–D). At the smallest fractional coverage studied, $\theta = 0.3$, the values are similar to or somewhat higher than for $\theta = 1$. At monolayer coverage, the H_2O molecules interact not only with the surfaces but develop organized networks of H-bonds with other water molecules parallel to the surfaces. At less than monolayer coverage, however, individual molecules are either isolated from each other or form small surface H-bonded clusters. In either case, they are less well embedded in H-bond networks and are thus more mobile than at the higher surface coverages. For instance, at the muscovite (0 0 1) surface, the calculated surface atomic density contour maps for $\theta = 0.31$ indicate that almost all the water molecules are adsorbed in or near the cavities in six-member rings, that they are clustered together (this figure is not shown and is similar to the density maps of the water molecules contributing to the first two peaks of the molecular density profiles), and that there is almost no H-bonding between these clusters (Wang et al., 2005b). This result is consistent with the suggestion that water molecules are more mobile at submonolayer coverages that was made on the basis of thermodynamic entropy calculations from water adsorption

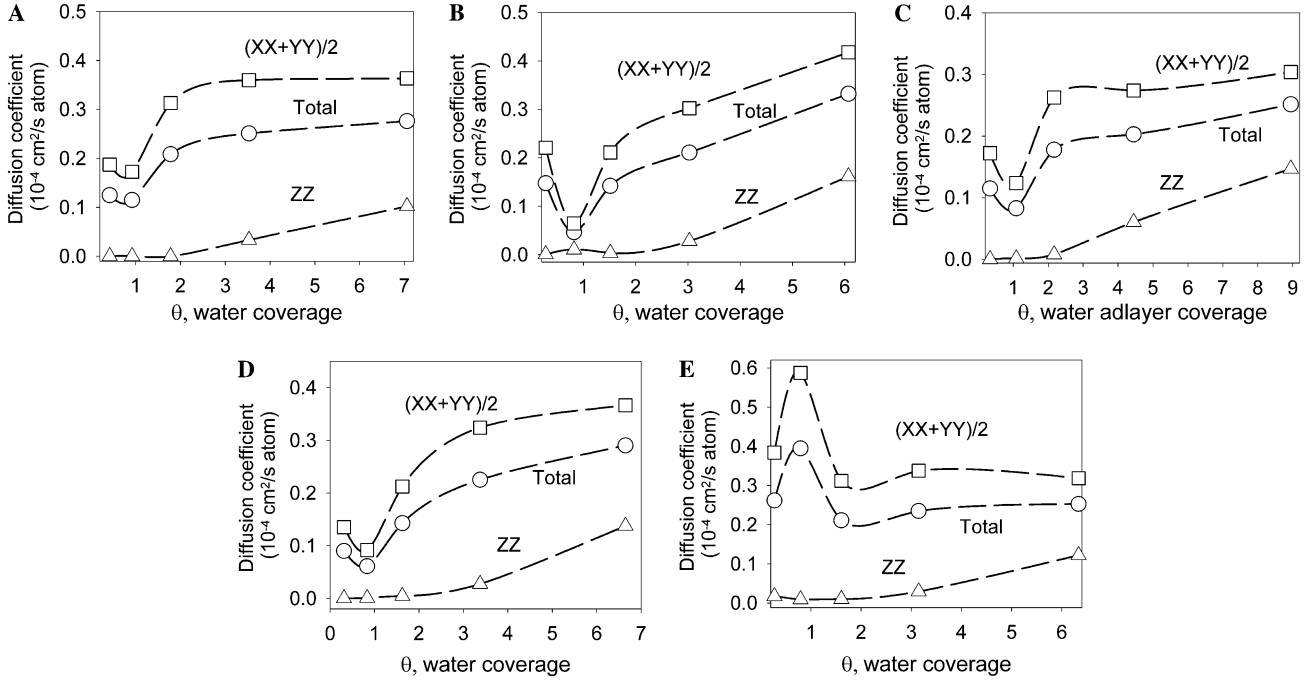

Fig. 6. Computed self-diffusion coefficients of interfacial O_{H_2O} as functions of water coverage, θ, for (A) brucite, (B) gibbsite, (C) hydrotalcite, (D) muscovite, and (E) talc. The values shown are the average diffusion coefficients of all water molecules present at a given coverage. The total diffusion coefficients (open circle) and the values perpendicular to (*ZZ*, open triangle) and parallel to (*XX* + *YY*, open square) the surfaces are shown separately. The dashed lines are eye guide.

experiments (Cantrell and Ewing, 2001), though no direct diffusion experimental work is available to either supports or disprove this notion. The atomic density maps for $\theta = 1.0$ show that H-bonding networks connect all the adsorbed water molecules and, thus, that cross-cluster H-bonding stabilizes the adsorbed water film. However, our 500 ps MD simulations show no interconnected two dimensional ice-like structures, as suggested from short-time (~2 ps) ab initio MD simulation (Odelius et al., 1997). Rather, our results show that even at a statistically monolayer coverage of $\theta = 1.0$, water molecules can diffuse as far as 7 Å from the surface and they are much more mobile than in ice. This is in agreement with vibrational spectroscopic measurements of adsorbed water at this coverage, which indicate that the adsorbed water structure is more liquid-like rather than ice-like (Cantrell and Ewing, 2001). Again, the ab initio MD simulation was performed for a duration of only 2 ps, and the short time of that simulation may have contributed to the stability of a well-ordered two-dimensional ice-like induced by the initial configuration. It is quite possible that only a relatively small region of the system's phase space in the vicinity of one of its local energy minima was probed. The H-bond life times and H_2O reorientation times of water molecules at hydrophilic surfaces are much longer (e.g., Ruan et al., 2004) than the total length of the simulation.

In contrast to the hydrophilic surfaces, the smallest computed total diffusion coefficient at the hydrophobic talc surface (Fig. 6E) occurs near $\theta = 2.0$, although here again, the XX and YY components are much greater than the ZZ component. This occurs because the interaction among water molecules is stronger than that between water molecules and the talc surface. Thus at near-monolayer coverage, the surface water molecules prefer to occur in large clusters or as isolated molecules and small clusters instead of in a monolayer film. The largest diffusion coefficient occurs near $\theta = 1.0$. At this coverage, water molecules form clusters that are smaller than those at higher coverages of $1.0 < \theta < 2.0$. These small clusters are much more mobile and behave more like molecular water clusters in the vapor phase (e.g., Kalinichev and Churakov, 2001; Kalinichev, 2001). Only at higher surface coverages ($\theta \sim 2.0$ for the talc–water interface) does the lateral interaction between these clusters become strong enough to connect them into a continuous lateral H-bonding network. Thus, at $\theta > 2.0$ the variation of the diffusion coefficients is very similar to those for the hydrophilic interfaces.

The reduced water self-diffusion coefficients observed here at hydrophilic surfaces are also observed for water molecules confined in the interlayers of LDH phases (Kagunya et al., 1997; Kalinichev et al., 2000; Kalinichev and Kirkpatrick, 2002) and some clay minerals (Smirnov and Bougeard, 1999; Greathouse et al., 2000). At the surfaces modeled here, the water molecules are confined to the surface film, whereas in the interlayers they are confined to a two-dimensional space. At the mineral surfaces, the reduced diffusion coefficients are due to interaction of H_2O with the surface via H-bonding and electrostatic interactions as well as lateral H-bonding interactions among the adsorbed water molecules. In the interlayers of clays and LDH phases, the water molecules interact with both confining charged surfaces, among themselves and with the charge-balancing anions or cations also present in the interlayers. The effects of the charged surfaces on the diffusional mobility of adsorbed water is analogous to the retarding effects that the electrostatic fields of strongly hydrated ions, such as Ca^{2+}, have on the dynamics of water molecules in their hydration shells, as observed in the MD simulations of bulk aqueous solutions (Bopp, 1987). The origin of the increased water self-diffusion coefficients at the hydrophobic talc (0 0 1) surface is less well understood and needs further theoretical and experimental investigation.

3.5. Hydration energetics of adsorbed water

The computational results show that substrate hydrophilicity/hydrophobicity and net structural charge have significant effects on the hydration energies that parallel those for the diffusivity (Fig. 7), and that the structural details such as surface interatomic distances and charge distribution are less important. For hydrophilic surfaces with no structural charge (brucite and gibbsite (0 0 1); Figs. 7A and B), the lowest hydration energy calculated according to Eq. (2) occurs at near monolayer water coverage, consistent with the stabilizing effects of H-bonding interaction with the surface and among water molecules at this coverage. The hydration energy at sub-monolayer coverages appears to be somewhat larger, but is, perhaps, the same within the statistical errors of our calculations. With increasing coverage at $\theta > 1$, the hydration energy (the average energy of all water molecules on the surface) increases and gradually approaches the value of the potential energy of one water molecule in bulk liquid SPC water (~10.1 ± 0.2 kcal/mol in our MD simulations). For the hydrophilic surfaces with net structural charge (hydrotalcite and muscovite; Figs. 7C and D), the hydration energy is the smallest at the lowest coverages and increases monotonically with water layer thickness. At $\theta < 1.0$, the electrostatic interaction between the charged surfaces and polar water molecules appears to play a dominant role. The fewer water molecules are on the surfaces, the stronger, on average, is the interaction of each of them with the surface. Although muscovite (0 0 1) has a somewhat larger charge density, $-0.022|e|/Å^2$, than hydrotalcite (0 0 1), $+0.019|e|/Å^2$, the higher hydration energy of Cl^- and the strong H-bonds between the water molecules and the hydrotalcite surface result in a much larger hydration energy per one H_2O molecule at this surface at $\theta < 1.0$ than at the same coverage for the muscovite surface. For the talc (0 0 1) surface (Fig. 7E), the calculated hydration energies decrease monotonically with increasing water coverage and gradually approach from above the bulk energy of SPC water. This relationship is consistent with the hydrophobic nature of talc and is the result of the interaction

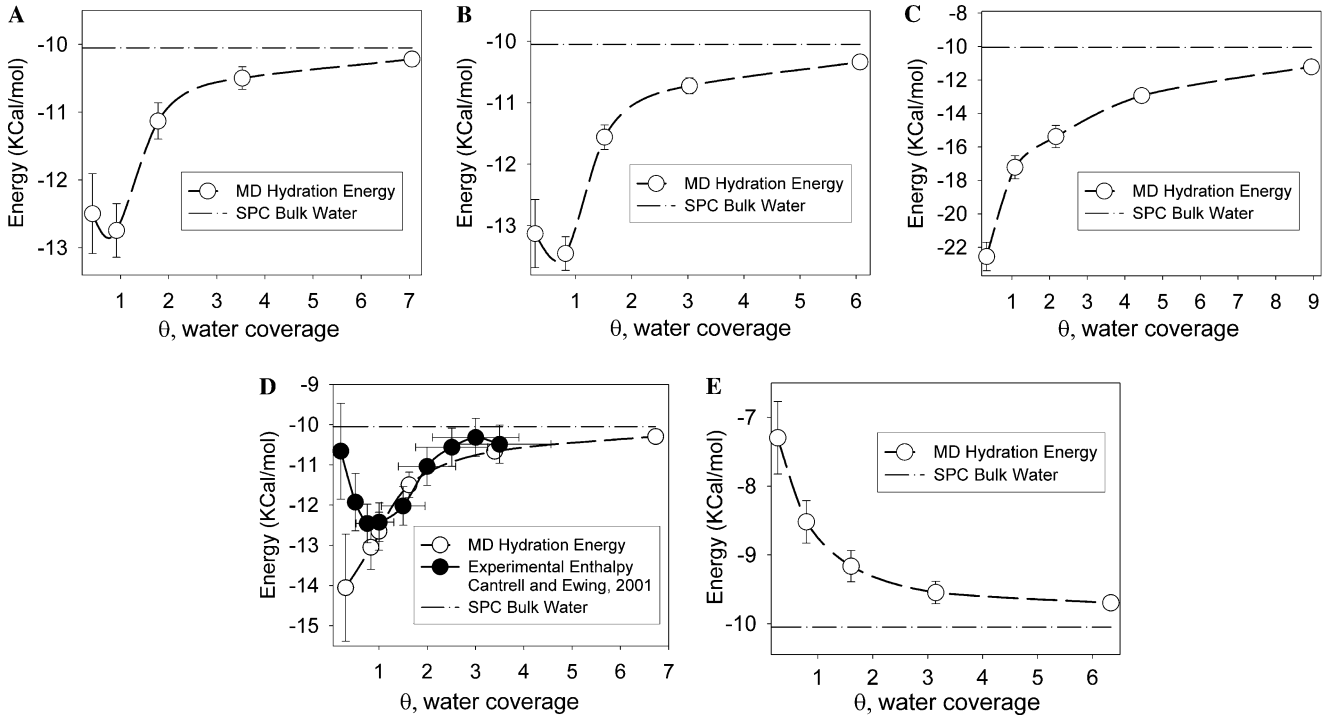

Fig. 7. Calculated energies of water adsorption on the modeled surfaces as functions of water coverage, θ, for (A) brucite, (B) gibbsite, (C) hydrotalcite, (D) muscovite, and (E) talc. Values shown represent the average energy of all molecules present on the surface at a given water coverage (see Eq. (2)). Error bars indicate one standard deviations of statistical mean. Error bars, if not shown, are within the symbols. Dashed lines are eye guide. The horizontal dot-dashed lines are hydration energy of SPC model at 300 K and density 1.0 g/cm^3 (−10.05 kcal/mol).

between water and talc (0 0 1) surface being weaker than that among water molecules themselves.

Our computed hydration energies show reasonably good quantitative agreement with other experimental and computed values. For water on the Al-hydroxide (0 0 1) surface of kaolinite, the interaction energy of a single water molecule with the surface is −8.3 kcal/mol based on the recent ab initio calculation (Tunega et al., 2002). Assuming that the interaction energy between water molecules on the surface at monolayer coverage is −5 kcal/mol, about half of the enthalpy of condensation of water at 298 K (−10.5 kcal/mol; Lide, 1999), the hydration energy at monolayer coverage would be −13.3 kcal/mol. This value is very close to the -13.5 ± 0.3 kcal/mol value from our MD calculations at the same coverage for gibbsite. For the tetrahedral (0 0 1) surface of kaolinite, following the same assumptions and using the single molecule value of −4.1 kcal/mol from Tunega et al. (2002), the estimated hydration energy of water at monolayer coverage is −9.1 kcal/mol, again in good agreement with the value of -8.8 ± 0.3 kcal/mol, from our MD simulations for talc (extrapolated from the Fig. 7E).

For water on the muscovite (0 0 1) surface, there is good agreement between the MD calculated hydration energies and the hydration enthalpies extracted from the experimental water adsorption data (Cantrell and Ewing, 2001) at $\theta > 1.0$, but poorer agreement at lower coverages (Fig. 7D). At $\theta = 1.0$, the hydration energy from our MD simulation is -12.6 K $\pm$ 0.5 kcal/mol, compared to the experimental value of -12.4 ± 0.5 kcal/mol (Cantrell and Ewing, 2001). The agreement at large coverages indicates that our model correctly evaluates the relative interaction energies between water molecules and the surface and among the water molecules themselves and that the $P\Delta V$ term can, indeed, be safely neglected for comparisons to the experimental enthalpy data at greater than a monolayer coverage.

At low surface coverages, $\theta < 1.0$, the sources of the discrepancy between the observed hydration enthalpies (Cantrell and Ewing, 2001) and the MD hydration energies may be either computational, or experimental. On the one hand, it is known that different water potentials may give slightly different hydration energies in bulk liquid (Jorgensen et al., 1983; Robinson et al., 1996; Engkvist and Stone, 2000; Jorgensen and Tirado-Rives, 2005; Vega et al., 2005), and thus our results, as for any other model, may be model-specific to some degree. Individual water molecules are more strongly perturbed on the surfaces at low coverage than at large coverage or in the bulk, thus, the difference on hydration energy could be even larger at the surfaces using different water potentials. Although the SPC model is known to perform very well for bulk liquid water (e.g., Robinson et al., 1996; Guillot, 2002) and overall seems to perform well for surface and confined water (Cygan et al., 2004a,b), it may not perform as well at the muscovite (0 0 1) surface.

On the other hand, it is known that the negatively charged, freshly cleaved muscovite (0 0 1) surface is

extremely chemically active (Beaglehole and Christenson, 1992), and any contamination from ambient lab air could neutralize active surface sites and strongly affect the experimentally measured adsorption enthalpies. A contaminated muscovite (0 0 1) surface might then behave more like a neutral one, similar to the surfaces of brucite or gibbsite as shown in Figs. 7A and B. The experimentally measured water adsorption enthalpies would be especially strongly dependent on such surface contamination effects at low coverages, $\theta < 1$, because under these conditions each H_2O molecule is adsorbed on the surface independently. If the last assumption is true, we might expect the hydration energy to be nearly constant, $[\partial(\Delta U_H)/\partial\theta]_{\theta<1} \approx 0$, which is inconsistent with both the experimental and calculated trends shown in 7D. However, the number of adsorbed water molecules is small at these coverages, and the statistical errors for both calculated and measured energies are especially large and hard to estimate accurately. Therefore, it is quite possible that a constant value of $\Delta U_H \approx -12.5$ kcal/mol would reasonably satisfy both sets of data at $\theta < 1$ (Fig. 7D).

4. Concluding remarks and geochemical implications

The MD simulation results presented here provide improved understanding on how mineral substrate structure and composition affect the molecular-scale structure and properties of interfacial water. The atomic density profiles of water perpendicular to the surface are largely controlled by the mineral surface structure. The orientations of these molecules, however, are dominantly influenced by surface hydrophobicity, surface charge distribution, and the ability to form H-bonds with adsorbed water molecules. The first molecular layers of water at all the surfaces are well ordered parallel to the surface, reflecting the substrate crystal structure and composition. This structure, however, is different from that of ice. The mobility of adsorbed water molecules and the enthalpy of surface hydration are controlled by mineral surface charge and hydrophobicity.

As with any modeling effort, the results are expected to be sensitive to details of the interatomic interaction potentials used. *CLAYFF* has been highly successful in simulating the crystal and interlayer structures of a wide variety of low-temperature oxide and hydroxide phases. To further test the sensitivity of the results here, we performed an additional MD simulation for water on the muscovite (0 0 1) surface with reduced charge on the basal oxygens, and essential conclusions are unaffected. In this simulation all surface basal oxygen atoms carried approximately 10% lower charges ($-1.1688|e|$ instead of $-1.05|e|$). Charge balance was obtained by adjusting the charges on the apical oxygen atoms of the Si,Al tetrahedral, and the other interaction parameters were unchanged. The O_{H_2O} and H_{H_2O} atomic density profiles and other structural and dynamic properties of the system showed minor quantitative differences but none of the changes affect the conclusions in any essential way. To eventually resolve the questions related to potential model-dependencies in MD simulations of natural systems, it will be necessary to undertake many more simulations using different potentials and ab inito MD calculations for at least select systems. Mutual comparison to the interpretations of experimental data for the structure of surface-associated fluids obtained by, for instance, spectroscopic methods and X-ray and neutron scattering will also be essential to advancing both experiment and theory. Such comparisons were key to the development of force fields for water and solute for bulk aqueous systems (see, e.g., Guillot, 2002 for a review). For instance, recent comparison of the diffusion coefficients of water on the surface of hydrous Ca-silicates obtained from ^{1}H NMR field cycling relaxation measurements and MD simulation are in good agreement. These results are expected to lead to the development of more advanced models of the surfaces of these complex phases. In addition, MD simulations of water on the muscovite (0 0 1) surface (Wang et al., 2005b) provide a highly detailed structure for mutual comparison to recent X-ray reflectivity measurements for the same system (Cheng et al., 2001). In their interpretations, Cheng et al. (2001) assumed that the first and all the subsequent surface water layers can be represented by a series of equally spaced Gaussian functions that broaden progressively from the surface. The MD results (Fig. 3) suggest that although this assumption could be reasonably accurate for non-polar molecules at a "hard wall" surface (e.g., Abraham, 1978) it may not be appropriate for the case of polar water molecules at the charged muscovite surface, because it oversimplifies the atomic density variation. Again, interactive comparison of the experimental and computational results will advance both.

Although the mineral–water interfaces considered here represent only a few idealized cases of perfect surfaces in contact with pure liquid water, detailed quantitative analysis of the effects of mineral substrate structure and composition on the structure, dynamics, and energetics of interfacial water within the framework of a single force field model are highly instructive, because the fundamental structural and dynamical conclusions seem to be quite robust and generalizable to systems containing mineral surfaces with similar compositions, structures, and net charges. For instance, comparison of experimental ^{35}Cl NMR results and MD-simulations show the importance of the orientation of the negatively charged (O) end of the water molecule towards the positively charged mineral surface in controlling the structure and dynamics of H_2O and Cl^- in the interlayers of the Ca,Al-layered double hydroxide, hydrocalumite (Kalinichev et al., 2000; Kalinichev and Kirkpatrick, 2002). These results are in excellent agreement with the results for hydrotalcite here. Similarly, for water on the surface of the hydrous Ca-silicate, tobermorite, recent MD simulations have shown the importance of mutual H-bond donation and acceptance between H_2O and surface Si–OH sites, analogous to the Mg–OH and Al–OH sites of brucite and gibbsite studied here. Such

mutual H-bond donation and acceptance between protonated surface sites and H_2O appears to be generally important at hydroxylated surfaces. In the future, incorporation of inorganic and organic solutes and mineral surface defects will bring the molecular models closer to the complex geochemical reality. Advanced, atomistically detailed surface specific experimental data will also be essential. These, of course, are subjects of future investigations. The progress in this direction would eventually provide a solid molecular-scale picture of aqueous mineral interfaces that should be complementary to the common macroscopic surface electric double layer models.

Acknowledgments

This research was supported by DOE Basic Energy Sciences Grant DEFGO2-00ER-15028 and the NSF Center of Advanced Materials for Water Purification with Systems (WaterCAMPWS) at the University of Illinois. Computations were partially supported by the National Computational Science Alliance (Grant EAR 990003N) and utilized NCSA SGI/CRAY Origin 2000 computers and Cerius2-4.5 software package from Accelrys. J. Wang also acknowledges a fellowship from the University of Illinois at Urbana-Champaign. Fruitful discussions with R.T. Cygan (Sandia National Lab, USA) concerning the *CLAYFF* forcefield parameterization are most gratefully acknowledged.

Associate editor: William H. Casey

References

Abraham, F.F., 1978. The interfacial density profile of a Lennard-Jones fluid in contact with a (100) Lennard-Jones wall and its relationship to idealized fluid/wall systems: A Monte Carlo simulation. *Journal of Chemical Physics* **68**, 3713–3716.

Accelrys, Inc., 2000. Cerius2-4.5. User's Guide. Forcefield-Based Simulations, San Diego.

Allen, M.P., Tildesley, D.J., 1987. *Computer Simulation of Liquids*. Clarendon Press, Oxford.

Akiyama, R., Hirata, F., 1998. Theoretical study for water structure at highly ordered surface: effect of surface structure. *Journal of Chemical Physics* **108**, 4904–4911.

Arab, M., Bougeard, D., Smirnov, K.S., 2003. Structure and dynamics of the interalyer water in an uncharged 2:1 clay. *Physical Chemistry Chemical Physics* **5**, 4699–4707.

Beaglehole, D., Christenson, H.K., 1992. Vapor adsorption on mica and silica: Entropy effect, layering, and surface forces. *Journal of Physical Chemistry* **96**, 3395–3403.

Bellotto, M., Rebours, B., Clause, O., Lynch, J., Bazin, D., Elkaim, E., 1996. A reexamination of hydrotalcite crystal chemistry. *Journal of Physical Chemistry* **100**, 8527–8534.

Beran, A., 2002. Infrared spectroscopy of mica. *Reviews in Mineralogy and Geochemistry* **46**, 351–369.

Berendsen, H.J.C., Postma, J.P.M., van Gunsteren, W.F., Hermans, J., 1981. Interaction models for water in relation to protein hydration. In: Pullman, B. (Ed.), *Intermolecular Forces*. Riedel, Dordrecht, The Netherlands, p. 331.

Boclair, J.W., Braterman, P.S., Brister, B.D., Yarberry, F., 1999. Layer–anion interactions in magnesium aluminum layered double hydroxides intercalated with cobalticyanide and nitroprusside. *Chemistry of Materials* **11** (8), 2199–2204.

Bopp, P., 1987. Molecular dynamics computer simulations of solvation in hydrogen bonded systems. *Pure and Applied Chemistry* **59**, 1071–1082.

Bopp, P.A., Heinzinger, K., 1998. MD studies of electrolyte solution/liquid mercury interfaces. *Journal of Electroanalytical Chemistry* **450**, 165–173.

Bridgeman, C.H., Buckingham, A.D., Skipper, N.T., Payne, M.C., 1996. Ab initio total energy study of uncharged 2:1 clays and their interaction with water. *Molecular Physics* **89**, 879–888.

Bridgeman, C.H., Skipper, N.T., 1997. A Monte Carlo study of water at an uncharged clay surface. *Journal of Physics: Condensed Matter* **9**, 4081–4087.

Brigatti, M.F., Guggenheim, S., 2002. Mica crystal chemistry and the influence of pressure, temperature, and solid solution on atomistic models. *Reviews in Mineralogy and Geochemistry* **46**, 1–97.

Brown, G.E., 2001. How minerals react with water. *Science* **294**, 67–70.

Brown, G.E., Henrich, V.E., Casey, W.H., Clark, D.L., Eggleston, C., Felmy, A., Goodman, D.W., Gratzel, M., Maciel, G., McCarthy, M.I., Nealson, K.H., Sverjensky, D.A., Toney, M.F., Zachara, J.M., 1999. Metal oxide surfaces and their interactions with aqueous solutions and microbial organisms. *Chemical Reviews* **99**, 77–174.

Brown, G.E., Parks, G.A., 2001. Sorption of trace elements on mineral surfaces: modern perspectives from spectroscopic studies, and comments on sorption in the marine environment. *International Geology Review* **43**, 963–1073.

Bryk, T., Haymet, A.D.J., 2002. Ice-Ih/water interface of the SPC/E model: molecular dynamics simulations of the equilibrium basal and prism interfaces. *Journal of Chemical Physics* **117**, 10258–10268.

Cai, H., Hillier, A.C., Franklin, K.R., Nunn, C.C., Ward, M.D., 1994. Nanoscale image of molecular adsorption. *Science* **266**, 1551–1555.

Cantrell, W., Ewing, G.E., 2001. Thin film water on muscovite mica. *Journal of Physical Chemistry B* **105**, 5434–5439.

Cheng, L., Fenter, P., Nagy, K.L., Schlegel, M.L., Sturchio, N.C., 2001. Molecular-scale density oscillations in water adjacent to a mica surface. *Physical Review Letters* **87**, 156103–156104.

Cygan, R.T., 2001. Molecular modeling in mineralogy and geochemistry. *Reviews in Mineralogy and Geochemistry* **42**, 1–35.

Cygan, R.T., Liang, J.-J., Kalinichev, A.G., 2004a. Molecular models of hydroxide, oxyhydroxide, and clay phases and the development of a general force field. *Journal of Physical Chemistry B* **108**, 1255–1266.

Cygan, R.T., Guggenheim, S., van Groos, A.F.K., 2004b. Molecular models for the intercalation of methane hydrate complexes in montmorillonite clay. *Journal of Physical Chemistry B* **108**, 15141–15149.

Davis, J.A., Kent, D.B., 1990. Surface complexation modeling in aqueous geochemistry. *Reviews in Mineralogy* **23**, 177–260.

Desgranges, L., Calvarin, G., Chevrier, G., 1996. Interlayer interactions in $M(OH)_2$: a neutron diffraction study of $Mg(OH)_2$. *Acta Crystallographica B* **52**, 82–86.

Dimitrov, D.I., Raev, N.D., Semerdzhiev, K.I., 2001. Molecular dynamics simulations of the electrical double layer at 1 M potassium halide/Hg electrode interfaces. *Physical Chemistry Chemical Physics* **3**, 448–452.

Du, Q., Freysz, E., Shen, Y.R., 1994. Vibrational spectra of water molecules at quartz water interfaces. *Physical Review Letters* **72**, 238–241.

Eisenberg, D., Kauzmann, W., 1969. *The Structure and Properties of Water*. Oxford University Press, Oxford.

Engkvist, O., Stone, A.J., 2000. Adsorption of water on the NaCl (001) surface. III. Monte Carlo simulations at ambient temperatures. *Journal of Chemical Physics* **112**, 6827–6833.

Errington, J.R., Debenedetti, P.G., 2001. Relationship between structural order and the anomalies of liquid water. *Nature* **409**, 318–321.

Fenter, P., Sturchio, N.C., 2004. Mineral–water interfacial structures revealed by synchrotron X-ray scattering. *Progress in Surface Science* **77**, 171–258.

Finney, J.L., 2001. The water molecule and its interactions: The interaction between theory, modelling, and experiment. *Journal of Molecular Liquids* **90**, 303–312.

Floris, F.M., Tani, A., 1999. Interaction potentials for small molecules. In: Balbuena, P.B., Seminario, J.M. (Eds.), *Molecular dynamics. From classical to quantum methods. Theoretical and Computational Chemistry*, vol. 7. Elsevier, Amsterdam, pp. 363–429.

Gallo, P., Rapinesi, M., Rovere, M., 2002. Confined water in the low hydration regime. *Journal of Chemical Physics* **117**, 369–375.

Greathouse, J.A., Refson, K., Sposito, G., 2000. Molecular dynamics simulation of water mobility in magnesium–smectite hydrates. *Journal of the American Chemical Society* **122**, 11459–11464.

Greathouse, J.A., Stellalevinsohn, H.R., Denecke, M.A., Bauer, A., Pabalan, R.T., 2005. Uranyl surface complexes in a mixed-charge montmorillonite: Monte Carlo computer simulation and polarized XAFS results. *Clays and Clay Minerals* **53**, 278–286.

Guillot, B., 2002. A reappraisal of what we have learnt during three decades of computer simulations on water. *Journal of Molecular Liquids* **101**, 219–260.

Güven, N., 1971. The crystal structures of 2M1 phengite and 2M1 muscovite. *Zeitschrift für Kristallographie* **134**, 196–212.

Head-Gordon, T., Hura, G., 2002. Water structure from scattering experiments and simulation. *Chemical Reviews* **102**, 2651–2669.

Henderson, M.A., 2002. The interaction of water with solid surfaces: fundamental aspects revisited. *Surface Science Reports* **46**, 1–308.

Hochella, M.F., White, A.F., 1990. Mineral–water interface geochemistry: an overview. *Reviews in Mineralogy* **23**, 1–16.

Israelachvili, J.N., Wennerström, H., 1996. Role of hydration and water structure in biological and colloidal interactions. *Nature* **379**, 219–225.

Jorgensen, W.L., Chandrasekhar, J., Madura, J.D., Impey, R.W., Klein, M.L., 1983. Comparison of simple potential functions for simulating liquid water. *Journal of Chemical Physics* **79**, 926–935.

Jorgensen, W.L., Tirado-Rives, J., 2005. Potential energy functions for atomic-level simulations of water and organic and biomolecular systems. *PNAS* **102**, 6665–6670.

Joseph, Y., Ranke, W., Weiss, W., 2000. Water on FeO(1 1 1) and Fe_3O_4(1 1 1): adsorption behavior on different surface terminations. *Journal of Physical Chemistry B* **104**, 3224–3236.

Kagunya, W., Dutta, P.K., Lei, Z., 1997. Dynamics of water in hydrotalcite. *Physica B* **234–236**, 910–913.

Kalinichev, A.G., 2001. Molecular simulations of liquid and supercritical water: thermodynamics, structure, and hydrogen bonding. *Reviews in Mineralogy and Geochemistry* **42**, 83–129.

Kalinichev, A.G., Churakov, S.V., 2001. Thermodynamics and structure of molecular clusters in supercritical water. *Fluid Phase Equilibria* **183**, 271–278.

Kalinichev, A.G., Kirkpatrick, R.J., 2002. Molecular dynamics modeling of chloride binding to the surfaces of Ca hydroxide, hydrated Ca-aluminate and Ca-silicate phases. *Chemistry of Materials* **14**, 3539–3549.

Kalinichev, A.G., Kirkpatrick, R.J., Cygan, R.T., 2000. Molecular modeling of the structure and dynamics of the interlayer and surface species of mixed-metal layered hydroxides: chloride and water in hydrocalumite (Friedel's salt). *American Mineralogist* **85**, 1046–1052.

Karaborni, S., Smit, B., Heidug, W., Urai, J., Oort, E.V., Urai, E., 1996. The swelling of clays: molecular simulations of the hydration of montmorillonite. *Science* **271**, 1102–1104.

Karim, O.A., Haymet, A.D.J., 1988. The ice/water interface: a molecualr dynamics simulation study. *Journal of Chemical Physics* **89**, 6889–6896.

Kirkpatrick, R.J., Kalinichev, A.G., Wang, J., Hou, X., Amonette, J.E., 2005a. Molecular modeling of the vibrational spectra of interlayer and surface species of layered double hydroxides. In: Kloprogge, J.T. (Ed.), *The Application of Vibrational Spectroscopy to Clay Minerals and Layered Double Hydroxides, CMS Workshop Lectures*, vol. 13. The Clay Minerals Society, pp. 239–285.

Kirkpatrick, R.J., Kalinichev, A.G., Wang, J., 2005b. Molecular dynamics modelling of hydrated mineral interlayers and surfaces: structure and dynamics. *Mineralogical Magazine* **69**, 289–308.

Kirkpatrick, R.J., Kalinichev, A.G., Hou, X., Struble, L., 2005c. Experimental and molecular dynamics modeling studies of interlayer swelling: water in kanemite and ASR gel. *Materials and Structures* **38**, 449–458.

Kuwahara, Y., 1999. Muscovite surface structure imaged by fluid contact mode AFM. *Physics and Chemistry of Minerals* **26**, 198–205.

Lee, S.H., Rossky, P.J., 1994. A comparison of the structure and dynamics of liquid water at hydrophobic and hydrophilic surface—a molecular dynamics simulation study. *Journal of Chemical Physics* **100**, 3334–3345.

Lide, R.D., 1999. *Handbook of Chemistry and Physics*. CRC Press, Boca Raton, FL.

Loewenstein, W., 1954. The distribution of aluminum in the tetrahedra of silicates and aluminates. *American Mineralogist* **39**, 92–96.

Luzar, A., 2000. Resolving the H-bond dynamics conundrum. *Journal of Chemical Physics* **113**, 10663–10675.

Masini, P., Bernasconi, M., 2002. Ab initio simulations of hydroxylation and dehydroxylation reactions at surfaces: amorphous silica and brucite. *Journal of Physics: Condensed Matter* **14**, 4133.

McCarthy, M.I., Schenter, G.K., Scamehorn, C.A., Nicholas, J.B., 1996. Structure and dynamics of the water/MgO interface. *Journal of Physical Chemistry* **100**, 16989–16995.

McKeown, D.A., Bell, M.I., Etz, E.S., 1999. Vibrational analysis of the dioctahedral mica: 2M1 muscovite. *American Mineralogist* **84**, 1041–1048.

Michot, L.J., Villiéras, F., Francois, M., Bihannic, I., Pelletier, M., Cases, J.-M., 2002. Water organization at the solid–aqueous solution. *C.R. Geoscience* **334**, 611–631.

Odelius, M., Bernasconi, M., Parrinello, M., 1997. Two dimensional ice adsorbed on mica surface. *Physical Review Letters* **78**, 2855.

Ohtaki, H., Radnai, T., 1993. Structure and dynamics of hydrated ions. *Chemical Reviews* **93**, 1157–1204.

Ostroverkhov, V., Waychunas, G.A., Shen, Y.R., 2004. Vibrational spectra of water at water/α-quartz (0 0 0 1) interface. *Chemical Physics Letters* **386**, 144–148.

Ostroverkhov, V., Waychunas, G.A., Shen, Y.R., 2005. New information on water interfacial structure revealed by phase-sensitive surface spectroscopy. *Physics Review Letters* **94**, 046102.

Park, S.-H., Sposito, G., 2002. Structure of water adsorbed on a mica surface. *Physics Review Letters* **89**, 085501.

Packer, K.J., 1977. The dynamics of water in heterogeneous systems. *Philosophical Transactions of the Royal Society of London, Series B: Biological Sciences* **278**, 59–87.

Rayner, J.H., Brown, G., 1973. The crystal structure of talc. *Clays and Clay Minerals* **21**, 103–114.

Robinson, G.W., Zhu, S.-B., Singh, S., Evans, M.W., 1996. *Water in Biology, Chemistry and Physics. Experimental Overviews and Computational Methodologies*. World Scientific, Singapore.

Rosenqvist, J., Persson, P., Sjöberg, S., 2002. Protonation and charging of nanosized gibbsite (α-$Al(OH)_3$) particles in aqueous suspension. *Langmuir* **18**, 4598–4604.

Ruan, C.Y., Lobastov, V.A., Vigliotti, F., Chen, S., Zewail, A.H., 2004. Ultrafast electron crystallography of interfacial water. *Science* **304**, 80–84.

Rustad, J.R., 2001. Molecular models of surface relaxation, hydroxylation, and surface charging at oxide–water interfaces. *Reviews in Mineralogy and Geochemistry* **42**, 169–197.

Rustad, J.R., Felmy, A.R., Bylaska, E.J., 2003. Molecular simulation of the magnetite–water interface. *Geochimica et Cosmochimica Acta* **67**, 1001–1016.

Saalfeld, H., Wedde, M., 1974. Refinement of the crystal structure of gibbsite, $Al(OH)_3$. *Zeitschrift für Kristallographie* **139**, 129–135.

Sakuma, H., Tsuchiya, T., Kawamura, K., Otsuki, K., 2003. Large self-diffusion of water on brucite surface by ab initio potential energy surface and molecular dynamics simulations. *Surface Science* **536**, L396–L402.

Scatena, L.F., Brown, M.G., Richmond, G.L., 2001. Water at hydrophobic surfaces: weak hydrogen bonding and strong orientation effects. *Science* **292**, 908–912.

Skipper, N.T., Soper, A.K., McConnell, J.D.C., 1991. The structure of interlayer water in vermiculite. *Journal of Chemical Physics* **94**, 5751–5760.

Smirnov, K.S., Bougeard, D., 1999. A molecular dynamics study of structure and short-time dynamics of water in kaolinite. *Journal of Physical Chemistry B* **103**, 5266–5273.

Smith, D.E., 1998. Molecular computer simulations of the swelling properties and interlayer structure of cesium montmorillonite. *Langmuir* **14**, 5959–5967.

Spohr, E., 1999. Molecular simulaiton of the electrochemical double layer. *Electrochimica Acta* **44**, 1697–1705.

Spohr, E., Hartnig, C., Gallo, P., Rovere, M., 1999. Water in porous glasses. A computer simulation study. *Journal of Molecular Liquids* **80**, 165–178.

Soper, A.K., 2000. The radial distribution functions of water and ice from 220 to 673 K and at pressures up to 400 MPa. *Chemical Physics* **258**, 121–137.

Stöckelmann, E., Hentschke, R., 1999. A molecular-dynamics simulation study of water on NaCl(001) using a polarizable model. *Journal of Chemical Physics* **110**, 12097–12107.

Terzis, A., Filippakis, S., Kuzel, H.-J., Burzlaff, H., 1987. The crystal structure of $Ca_2Al(OH)_6Cl\cdot 2H_2O$. *Zeitschrift für Kristallographie* **181**, 29–34.

Teschke, O., Ceotto, G., de Souza, E.F., 2000. Interfacial aqueous solutions dielectric constant measurements using atomic force microscopy. *Chemical Physics Letters* **326**, 328–334.

Thiel, P.A., Madey, T.E., 1987. The interaction of water with solid surfaces: fundamental aspects. *Surface Science Reports* **7**, 211–385.

Trainor, T.P., Chaka, A.M., Eng, P.J., Newville, M., Waychunas, G.A., Catalano, J.G., Brown, G.E., 2004. Structure and reactivity of the hydrated hematite (001) surface. *Surface Science* **573**, 204–224.

Tunega, D., Gerzabek, M.H., Lischka, H., 2004. Ab initio molecular dynamics study of a monomolecular water layer on octahedral and tetrahedral kaolinite surfaces. *Journal of Physical Chemistry B* **108**, 5930–5936.

Tunega, D., Haberhauer, G., Gerzabek, M.H., Lischka, H., 2002. Theoretical study of adsorption sites on the (001) surfaces of 1:1 clay minerals. *Langmuir* **18**, 139–147.

Vega, C., Sanz, E., Abascal, J.L.F., 2005. The melting temperature of the most common models of water. *Journal of Chemical Physics* **122**, 114507.

Vucelic, M., Jones, W., Moggridge, G.D., 1997. Cation ordering in synthetic layered double hydroxides. *Clays and Clay Minerals* **45**, 803.

Wallqvist, A., Mountain, R.D., 1999. Molecular models of water: derivation and description. In: Lipkowitz, K.B., Boyd, D.B. (Eds.), *Reviews in Computational Chemistry*, vol. 13. Wiley/Wiley–VCH, New York, pp. 183–247.

Wang, J., Kalinichev, A.G., Amonette, J.E., Kirkpatrick, R.J., 2003. Interlayer structure and dynamics of Cl-hydrotalcite: far infrared spectroscopy and molecular dynamics modeling. *American Mineralogist* **88**, 398–409.

Wang, J., Kalinichev, A.G., Kirkpatrick, R.J., 2004a. Molecular modeling of the 10-Å phase at subduction zone conditions. *Earth and Planetary Science Letters* **222**, 517–527.

Wang, J., Kalinichev, A.G., Kirkpatrick, R.J., 2004b. Molecular modeling of water structure in nano-pores between brucite (001) surfaces. *Geochimica et Cosmochimica Acta* **68**, 3351–3365.

Wang, J., Kalinichev, A.G., Kirkpatrick, R.J., 2005a. Structure and decompression melting of a novel, high-pressure nanoconfined 2-D ice. *Journal of Physical Chemistry B* **109**, 14308–14313.

Wang, J., Kalinichev, A.G., Kirkpatrick, R.J., Cygan, R.T., 2005b. Structure, energetics, and dynamics of water adsorbed on the muscovite (001) surface: a molecular dynamics simulation. *Journal of Physical Chemistry B* **109**, 15893–15905.

Wang, J.W., Kalinichev, A.G., Kirkpatrick, R.J., Hou, X.Q., 2001. Molecular modeling of the structure and energetics of hydrotalcite hydration. *Chemistry of Materials* **13**, 145–150.

Wang, S.-L., Johnston, C.T., 2000. Assignment of the structural OH stretching bands of gibbsite. *American Mineralogist* **85**, 739–744.

Whitley, H.D., Smith, D.E., 2004. Free energy, energy, and entropy of swelling in Cs-, Na-, and Sr-montmorillonite clays. *Journal of Chemical Physics* **120**, 5387–5395.

Williams, G.D., Soper, A.K., Skipper, N.T., Smalley, M.V., 1998. High-resolution structural study of an electrical double layer by neutron diffraction. *Journal of Physical Chemistry B* **102**, 8945–8949.

Yao, K., Taniguchi, M., Nakata, M., Takahashi, M., Yamagishi, A., 1998. Nanoscale image of molecular adsorption of metal complexes on the surface of a hydrotalcite crystal. *Langmuir* **14**, 2410–2414.

Yeganeh, M.S., Dougal, S.M., Pink, H.S., 1999. Vibrational spectroscopy of water at liquid/solid interfaces: crossing the isoelectric point of a solid surface. *Physical Review Letters* **83**, 1179–1182.

Yu, C.-J., Richter, A.G., Datta, A., Durbin, M.K., Dutta, P., 1999. Observation of molecular layering in thin liquid films using X-ray reflectivity. *Physical Review Letters* **82**, 2326–2329.